

The benefits of increasing resolution in global and regional climate simulations for European climate extremes

Carley E. Iles¹, Robert Vautard¹, Jane Strachan², Sylvie Joussaume¹, Bernd R. Eggen² and Chris D. Hewitt²

¹Laboratoire des Sciences du Climat et de l'Environnement, LSCE-IPSL, CEA-CNRS-UVSQ, Université Paris-Saclay, F-91198 Gif-sur-Yvette, France

²Hadley Centre, Met Office, Exeter, UK

Correspondence to: Carley E. Iles (carley.iles@lsce.ipsl.fr)

Abstract. Many climate extremes, including heatwaves and heavy precipitation events, are projected to worsen under climate change, with important impacts for society. Future projections, required for adaptation, are often based on climate model simulations. Given finite resources, trade-offs must be made concerning model resolution, ensemble size and level of model complexity. Here we focus on the resolution component. A given resolution can be achieved over a region using either global climate models (GCMs) or at lower cost using regional climate models (RCMs) that dynamically downscale coarser GCMs. Both approaches to increasing resolution may better capture small-scale processes and features (downscaling effect), but increased GCM resolution may also improve the representation of large-scale atmospheric circulation (upscaling effect). The size of this upscaling effect is therefore important for deciding modelling strategies. Here we evaluate the benefits of increased model resolution for both global and regional climate models for simulating temperature, precipitation and wind extremes over Europe at resolutions that could currently be realistically used for coordinated sets of climate projections at the pan-European scale. First we examine the benefits of regional downscaling by comparing EURO-CORDEX simulations at 12.5 and 50 km resolution to their coarser CMIP5 driving simulations. Secondly, we compare global scale HadGEM3-A simulations at three resolutions (130, 60 and 25 km). Finally, we separate out resolution dependent differences for HadGEM3-A into downscaling and upscaling components using a circulation analogue technique. Results suggest limited benefits of increased resolution for heatwaves, except in reducing hot biases over mountainous regions. Precipitation extremes are sensitive to resolution, particularly over complex orography, with larger totals and heavier tails of the distribution at higher resolution, particularly in the CORDEX vs CMIP5 analysis. CMIP5 models underestimate precipitation extremes, whilst CORDEX simulations overestimate compared to E-OBS, particularly at 12.5 km, but results are sensitive to the observational dataset used, with the MESAN reanalysis giving higher totals and heavier tails than E-OBS. Wind extremes are somewhat stronger and heavier tailed at higher resolution, except at coastal regions where large coastal grid boxes spread strong ocean winds further over land. The circulation analogue analysis suggests that differences with resolution for the HadGEM3-A GCM are primarily due to downscaling effects.

34 **1 Introduction**

35 Climate extremes, such as heatwaves and heavy precipitation events are projected to worsen under climate change,
36 with important impacts for society (Seneviratne et al., 2012). Such projections are generally based on numerical
37 climate model simulations. However, given finite computational resources, trade-offs between model resolution,
38 ensemble size and the level of model complexity are necessary. For extreme events driven by large-scale processes
39 such as stationary anticyclones, the proper simulation of the amplitude of extremes is limited by dynamics but also
40 by land-atmosphere feedbacks and the many physical processes involved in the surface energy budget. Such
41 extremes are typically heat waves, droughts and cold spells. Many other types of extreme event are by nature small
42 scale, i.e. on the order of a few kilometres to a few hundred kilometres. Such is the case of convective precipitation,
43 flash floods, extratropical wind storms, cyclones and medicanes. These are poorly resolved at the resolution of
44 Global Climate Models (GCMs) in CMIP5 (Coupled Model Intercomparison Project Phase 5; Taylor et al., 2012).
45 Increased resolution in GCMs may improve the representation of small-scale processes and features, including
46 orography and coastlines (downscaling effect), but potentially may also improve the representation of the interaction
47 between small and large scale dynamical processes and ultimately improve the large-scale atmospheric flow
48 (upscaling effect). For instance, a better representation of baroclinic eddies may help to better simulate large Rossby
49 waves such as those inducing long-lived anomalies, due to the inverse energy cascade. This may improve the
50 simulation of the frequency and duration of heat waves and cold spells, and related anomalies such as summer
51 droughts. For precipitation and wind extremes, an improvement with resolution could be expected due to the small-
52 scale processes and features involved, including convection and the influence of topography. However, upscaling
53 effects may also have benefits by improving storm-track location, and duration of wet spells. An alternative approach
54 to increasing the resolution of global-scale models is to use regional climate models (RCMs) driven by coarser
55 GCMs to achieve a given high resolution over a limited area at lower cost. However, this technique only captures
56 downscaling effects, since the RCM inherits the large scale circulation from the driving GCM.

57
58 Current generation GCMs commonly used for climate projections (e.g. CMIP5 models) have a horizontal grid
59 spacing ranging from about 70 to 250 km, although 25 km GCMs are starting to be run under projects such as
60 PRIMAVERA and HighResMIP (part of CMIP6; Haarsma et al., 2016). For coordinated RCM experiments, such as
61 CORDEX (Coordinated Regional Downscaling Experiment; Giorgi et al., 2009), grid spacing is generally between
62 10 to 50 km (e.g. Jacob et al., 2014). In order to simulate convective precipitation a grid spacing of <5 km is needed,
63 which is very computationally expensive, but such ensembles of convection permitting RCMs are currently in
64 development (e.g. Coppola et al., 2019; Risanto et al. 2019). An important question is the extent to which increased
65 resolution benefits the simulation of extreme events for both global and regional models for the kind of resolutions
66 that can realistically be run for coordinated pan-continental climate projections. Particularly, whether using global
67 high resolution adds further benefits over regional high resolution due to an improved large scale circulation. We
68 will address these questions focusing on Europe, for which a large number of coordinated RCM simulations at two
69 standard resolutions are available as part of the EUROCORDEX project (Jacob et al., 2014, and whose climate is
70 highly variable and affected by a range of both large and small scale processes, which present challenges for

71 adequate simulation. We focus on extreme precipitation, temperature and wind, to cover a range of events that may
72 be affected by resolution in different ways. Throughout the rest of this manuscript we use the term “resolution” to
73 mean model horizontal grid spacing, whilst recognising that a model’s effective resolution, in terms of the scales it
74 can capture, is always less than its grid spacing (Skamarock 2004; Klavar et al. 2020).

75
76 The benefits of increased resolution for European precipitation extremes are well documented, whilst the effects on
77 heatwaves, cold spells and wind extremes are less well known. In GCMs, global precipitation tends to increase with
78 resolution, and for grid point models the fraction of land precipitation and moisture fluxes from land to ocean
79 increases, largely due to better resolved orography (Vannière et al., 2019; Terai et al., 2018; Demory et al., 2014).
80 Precipitation extremes tend to get heavier and agree better with observations (Wehner et al., 2010, O’Brien et al.,
81 2016; Kopparla et al., 2013; Shields et al., 2016; Vannière et al., 2019), unless the parameterisation schemes are not
82 suited to the resolution (e.g. Wehner et al., 2014). In Europe, Schiemann et al. (2018) find that both mean and
83 extreme precipitation are simulated better with increased resolution in HadGEM3A, mostly originating from better
84 resolved orography. In contrast, Van Haren et al. (2015a) find that improvements in Northern and Central European
85 mean and extreme winter precipitation with resolution are mostly associated with improved storm tracks in EC-
86 Earth. For RCMs, extreme precipitation is improved with resolution when compared to high resolution observations,
87 particularly over orography, including frequency-intensity distributions and spatial patterns, (see e.g. Torma et al.,
88 2015 and Prein et al., 2016 for EURO-CORDEX at 12.5 km vs 50km and vs the driving GCMs, and Ruti et al.,
89 (2016) for Med-CORDEX). However, benefits are smaller for regional and seasonal mean precipitation. Convection
90 permitting models (<4km grid spacing) are particularly beneficial in simulating summer extreme and sub-daily
91 precipitation, including the diurnal cycle of convection, but can overdo extreme precipitation (e.g. Prein et al., 2015;
92 Kendon et al., 2012; 2014).

93
94 For heatwaves, increasing horizontal resolution does not lead to obvious benefits in RCM simulations (see e.g.
95 Vautard et al., 2013 for EURO-CORDEX), except improved spatial detail (Gutjahr et al., 2016). However, increased
96 resolution may have more impact in global models since the large scale circulation that contributes to heatwave
97 formation may be affected. This remains a largely unstudied question, with the exception of a few studies such as
98 Cattiaux et al. (2013) who find that increasing resolution in the IPSL GCM leads to a reduction in the cold bias of
99 both cold and warm extremes in Europe, along with improved statistics, such as duration and frequencies and
100 improved weather regimes.

101
102 For wind extremes, stronger winds and better spatial detail with resolution have been found for regional models (e.g.
103 Pryor et al., 2012; Kunz et al., 2010). Donat et al. (2010) found that observed storm loss estimates for Germany
104 could be reconstructed more accurately through dynamical downscaling compared to using the coarser resolution
105 driving ERA-40 data directly. Ruti et al., (2016) found improvements in Mediterranean cyclogenesis in coupled
106 Med-CORDEX RCMs relative to the ERA-interim driving data, whilst extreme winds over the Mediterranean
107 generally improve (i.e. are stronger) with higher resolution RCMs (e.g. Ruti et al. 2016; Hermann et al. 2011).
108 However, most GCM studies focus on the simulation of extratropical cyclones rather than wind directly. Such

109 studies find an improvement in the representation of various aspects of Northern Hemisphere extratropical cyclones
110 with increased resolution, including frequency, intensity and the position of the storm tracks (Colle et al., 2013; Jung
111 et al., 2006; 2012), even in the higher resolution CMIP5 models (\sim <130 km; Zappa et al., 2013). Vries et al., (2019)
112 found that the resolution of Atlantic Gulf-Stream SST fronts affects winter extratropical cyclone strength. Whether
113 these improvements translate into an improvement in wind extremes remains to be assessed.

114
115 Persistence of weather regimes, such as blocking or the phase of the North Atlantic Oscillation, can be important
116 drivers for extreme events in Europe. Using the ECMWF IFS model, Dawson et al., (2012; 2015) find that such
117 weather regimes cannot be simulated realistically at typical CMIP5 resolution (\sim 125 km grid spacing), but are
118 improved at 40 km, and well-simulated at 16 km. Cattiaux et al., (2013) find improvements at more modest
119 resolutions in the IPSL model. Blocking frequency tends to be underestimated by CMIP5-resolution climate models
120 (Anstey et al., 2013). This tends to be improved with resolution, particularly over the North Atlantic (Jung et al.,
121 2012, Anstey et al., 2013; Matsueda et al., 2009, Berckmans et al., 2013, Davini et al., 2017a; 2017b), although
122 results tend to be somewhat sensitive to season and model considered (Schiemann et al., 2017) and compensating
123 errors may be involved (Davini et al., 2017a for EC-EARTH). O'Reilly et al. (2016) find that having a well-resolved
124 Gulf stream SST front is also important for European winter blocking and associated cold spells. An important
125 question is whether these improvements in the large scale circulation translate into an improvement in the simulation
126 of European climate extremes.

127
128 Here we examine the benefits of increased resolution for global models compared to regional models for the
129 simulation of European heatwaves, heavy precipitation events and wind storms. We further break down any
130 resolution related differences for a global model into upscaling and downscaling components. This will shed light on
131 whether potential improvements in the large scale circulation suggested in the literature translate into an improved
132 representation of climate extremes. This is an important consideration in choosing how to distribute finite resources
133 between global and regional models. We focus on the kind of models widely used to provide climate projections at a
134 European scale, applying a consistent approach across model types. Firstly, the benefits of regional dynamical
135 downscaling are explored by comparing EURO-CORDEX simulations at 50 and 12.5 km resolutions to their coarser
136 driving CMIP5 GCMs. Secondly, the benefits of increased resolution for a global model are examined using
137 HadGEM3-A at 130, 60 and 25 km resolution. Finally, the roles of upscaling versus downscaling will be examined
138 using a circulation analogue technique applied to HadGEM3-A.

139 **2 Observational and model data**

140 **2.1 Observations**

141 Model simulations are evaluated using observational and reanalysis datasets. For daily precipitation and daily
142 maximum temperature, we use the gridded station based dataset E-OBS on a 0.5° latitude-longitude grid (Haylock et
143 al. 2008). This covers the European domain from 1950 to present. Gridded datasets tend to reduce the magnitude of

144 extremes compared to station data through smoothing effects, but are more comparable to the grid box averages from
145 GCMs (Haylock et al. 2008). E-OBS has a somewhat non-uniform underlying station density, with relatively high
146 densities in Germany, Sweden and Slovenia, and low densities in other countries (e.g. Spain, France, Austria). It
147 tends to underestimate precipitation extremes relative to higher density regional datasets, especially where it has poor
148 coverage, due to missed extremes which are local in scale (Prein and Gobiet 2017). However, such high resolution
149 datasets are not available at a pan-European scale. As a compromise, results are repeated for precipitation extremes
150 using the 5.5 km resolution MESAN reanalysis (Landelius et al. 2016), which adjusts a downscaled first guess from
151 the 22km resolution HIRLAM reanalysis (Dahlgren et al. 2016) with a network of station-based precipitation
152 observations. For much of Europe these are the same as those used for E-OBS, but with the addition of Swedish
153 Meteorological and Hydrological Institute (SMHI) stations over Sweden, and a high density of Meteo-France
154 stations over France (Landelius et al. 2016). MESAN provides daily precipitation data for the more limited period
155 1989-2010. Prein and Gobiet (2017) find that it gives heavier extremes than E-OBS in some regions (France, Spain,
156 the Carpathians), but generally not as high as the high resolution regional datasets (except in France). Neither dataset
157 is corrected for gauge undercatch, which tends to be around 3-20% for rain, and up to 40% for snow, or even 80%
158 for non-shielded gauges (Førland and Institutt 1996; Goodison et al. 1997).

159
160 Wind extremes tend to happen on sub-daily time scales, necessitating the use of sub-daily data to avoid missing as
161 many events (although events, or their peak magnitude, will still be missed). We use 10 m wind speed from three
162 reanalysis datasets. These are the EURO4M DYNAD (Landelius et al. 2016), UERRA MESCAN-SURFEX (Bazile
163 et al. 2017) and ERA5 (Hersbach et al. 2019) reanalyses. The former is available at 6 hourly intervals on a 5.5km
164 rotated grid over Europe for the period 1979-2013 and is computed through dynamical adaptation a downscaled
165 version of the 22km resolution HIRLAM reanalysis to 5.5 km resolution orography using DYNAD (a simplified
166 version of HIRLAM). MESCAN is also available at the same spatial and temporal resolution over Europe from 1961
167 onwards, but is computed through dynamical downscaling of the 11 km UERRA-HARMONIE reanalysis. Both
168 HIRLAM and UERRA-HARMONIE are forced by the ERA interim global reanalysis (ERA40 before 1979 for the
169 latter). Finally, ERA5 is available globally at 0.25° and at hourly resolution from 1979 onwards. We sub-sample
170 ERA5 to 6 hourly data in order to be consistent with the other reanalyses.

171

172 **2.2 Climate model data**

173 **2.2.1 EURO-CORDEX and CMIP5**

174 In order to examine the effect of dynamical downscaling for climate extremes, we make use of the EURO-CORDEX
175 (Jacob et al. 2014) RCM simulations for the historical period over the European domain which are driven by lower
176 resolution global scale coupled CMIP5 GCMs. The GCMs are forced by observed records of anthropogenic and
177 natural forcings, such as greenhouse gases, anthropogenic aerosols, land use changes, solar variability and volcanic
178 aerosols to allow comparability to historical records. For the most part the RCMs inherit the effects of these forcing
179 agents from the GCMs, with the exception of greenhouse gases, which are prescribed. A comparison of the RCM

180 simulations with their driving CMIP5 simulations allows us to identify any value added by regional high resolution.
181 The EURO-CORDEX simulations are available at 0.11° and 0.44° (12.5 km and 50 km respectively), allowing an
182 assessment of the difference that increased regional resolution brings. By examining the subset of GCM-RCM
183 combinations that are common to both CORDEX resolutions along with their driving GCMs we can isolate the
184 effects of changing resolution.

185
186 Daily precipitation (pr), daily maximum temperature (tasmax), and daily maximum surface wind speed
187 (sfcWindmax) were taken from both CORDEX and CMIP5. The simulations used are shown in Table S1. These
188 consist of 23 and 19 simulations for precipitation for the 0.44° and 0.11° simulations respectively, with 15 common
189 to both categories with data also available from their driving GCMs (from now on referred to as “common to all” or
190 “common subset”); 22 and 18 respectively for temperature, with 14 common to all, and 15 and 14 for wind with 6
191 that are common to all. We also extend the analysis to all other historical CMIP5 GCMs with the relevant variables,
192 with 126 simulations from 41 GCMs for precipitation, 115 from 39 models for temperature and, 61 simulations from
193 28 models for wind. For wind, using 3 or 6 hourly data would have made results more comparable to the reanalysis
194 wind datasets and across models (see above). However, such data were not available for the 0.44° CORDEX
195 simulations, and very limited for CORDEX 0.11°. We therefore use the variable sfcWindmax (daily maximum
196 surface wind speed) which was available for many models. This seems to mostly be based on model timestep wind
197 speed, with a few exceptions (see figure S7). The implications of this are discussed further in the results section.

198 **2.2.2 UPSCALE simulations**

199 In order to examine the benefits or otherwise of differences in resolution for a global model, we make use of
200 simulations undertaken as part of the UPSCALE project (UK on PRACE: weather-resolving Simulations of Climate
201 for globAL Environmental risk; Mizielinski et al. 2014). This consists of the atmosphere only version of the Hadley
202 Centre Global Environment Model 3 (HadGEM3-A) run at three different resolutions: N96 (130 km), N216 (60 km)
203 and N512 (25 km), all with 85 vertical levels for the period 1985-2011, with 5, 3 and 5 ensemble members
204 respectively (or 3, 3 and 5 for wind data). The simulations are forced by observed records of greenhouse gases,
205 aerosols, ozone, solar variability and volcanic forcings following the AMIP-II procedure (Taylor et al. 2000), but
206 using the higher resolution OSTIA analysis for sea surface temperatures (SSTs) and sea ice (Donlon et al. 2012).
207 Very few parameters differ between the resolutions, enhancing the comparability of the three ensembles. We use
208 daily precipitation data, daily maximum temperatures and 3-hourly wind (subsampled to 6-hourly).

209 **2.2.3 Regridding**

210 In order to compare models of different resolutions with each other and with observations it was necessary to regrid
211 variables to a common grid. Using a high resolution grid for evaluation would preserve the finer spatial detail and
212 localised extremes for high resolution simulations, but is sometimes considered unfair for coarse resolution models
213 which cannot be expected to simulate the same intensities of extremes even for a perfect simulation due to spatial
214 smoothing effects (Prein et al. 2016). However, the finer spatial detail is an inherent advantage of high resolution and

215 smoothing this out will result in information loss. We use a 0.5° regular longitude-latitude grid since it is in-between
216 the resolution of the CORDEX models and CMIP5, is computationally feasible and E-OBS is also available at this
217 resolution. Some of the benefits of higher resolution may be lost by doing this, putting our results on the
218 conservative side. Nevertheless, sensitivity tests showed that results for MESAN did not change perceptibly by using
219 a 0.5° grid compared to a 0.1° grid. We regrid the daily data, before the calculation of annual extreme indices.

220
221 Sensitivity of results to regridding technique was investigated for a number of models of different resolutions and
222 compared with results based on using the original grids (Figure S1). For the coarser resolution models (e.g.
223 HadCM3) results for precipitation extremes were particularly sensitive to regridding technique, with much weaker
224 extremes for some techniques e.g. distance-weighted average remapping and bilinear interpolation, with unrealistic
225 artefacts in the spatial patterns for many methods. For high resolution models, regridding technique did not make
226 much difference to results, although conservative remapping tended to dampen extreme precipitation, particularly for
227 CORDEX 0.11. Overall the nearest neighbour method was chosen for precipitation for everything except CORDEX
228 0.11 and MESAN since it gave results very close to using the original grid for all model resolutions, preserving the
229 amplitude of extremes, and also having minimal artefacts when plotting spatial patterns of precipitation extremes.
230 For going from high to lower resolution (e.g. 0.11° to 0.5°) nearest neighbour is less appropriate since information
231 from only a subset of grid cells is incorporated. Therefore, bicubic remapping was used for CORDEX 0.11 and
232 MESAN, which also replicated results using the original grid very well (Figure S1). Wind and temperature results
233 were also somewhat sensitive to regridding technique, particularly for the coarser models. The above choices also
234 seemed appropriate for these variables (nearest neighbour in most cases, but bicubic for CORDEX 0.11, MESCAN,
235 ERA5 and DYNAD), both in terms of replicating return period results using the original grid, and retaining the
236 blocky nature of the low resolution simulations in the spatial patterns.

237 **3 Methods**

238 **3.1 Extremes Indices**

239 In order to examine extremes, we adopt indices based on the ETCCDI indices (Zhang et al. 2011). For precipitation
240 these are the annual maximum daily precipitation (Rx1day) and the annual maximum consecutive 5-day total
241 (Rx5day). For temperature we use the annual maximum daily maximum temperature (TXx) and the annual
242 maximum consecutive 5-day mean of daily maximum temperature (TXx5day). Rx1day and TXx5day are presented
243 in the figures, whilst the other indices are commented on in the text. For wind we use the annual maximum of daily
244 maximum wind, which we refer to as (WindXx). This is based on sfcWindmax for the CMIP5 and CORDEX
245 models, and on 6-hourly data for the UPSCALE simulations and the reanalysis wind datasets. These are therefore
246 much rarer extremes than those based e.g. on the 95th or even 99th percentile which would happen on average 1 in 20
247 days and 1 in 100 days respectively. One drawback is that this makes robust statistics more challenging.

248

249 In order to examine how well the climate models simulate extremes and the differences between different
250 resolutions, we first examine the spatial patterns of the climatological mean values of the indices and their biases
251 with respect to observations. We then examine return period plots (see definitions below) for a number of regions for
252 each index, which highlights any differences in the shape of the tails of the distribution of the extremes. The regions
253 used are based on the PRUDENCE regions (Christenson and Christenson 2007) and the IPCC SREX regions
254 (Seneviratne et al. 2012) and are shown in Figure S2 and Table S2. A subset of representative regions are presented
255 here, with some comments about the others.

256 **3.2 Return periods**

257 In order to calculate regional return periods and return values we first sort the data into ascending order for each grid
258 cell. The return periods are calculated as N/k where N is the number of years of data, and k is the rank, with $k=1$ for
259 the largest value. Return periods are therefore the inverse of the probability of an event exceeding a given value
260 (called the “return value”). The area weighted regional average is made, for given return periods, over the associated
261 return values. To avoid complications from missing data, grid cells in E-OBS with more than 5 days of missing data
262 in any year during the period examined were masked for the whole period. Having one or more years missing would
263 complicate the calculation of regional mean return periods and values. Models and observational datasets are masked
264 to have the same spatial coverage, which is land only. A common time period, across the models being examined and
265 the observations they are being compared to, are chosen to allow comparability. For the CMIP5 and CORDEX
266 analysis 1970-2005 is used for temperature and precipitation and 1979-2005 for wind. For the UPSCALE runs we
267 use 1985-2011 for temperature, and 1989-2010 for precipitation to allow comparisons with MESAN (1986-2011 is
268 used for the analogue analysis, see below) and 1986-2011 for wind.

269
270 In order to allow comparability of results between the EURO-CORDEX ensembles at both resolutions and their
271 driving CMIP5 GCMs, we picked a subset of models that are consistent across each category; that is the same GCM-
272 RCM combinations are used across both the 0.11 and 0.44° CORDEX categories, and are compared to the CMIP5
273 model runs that were used to drive them (Table S1). We refer to these simulations as the “common subset” (see
274 section 2.2.1). The only exception is that the EC-EARTH ensemble member “r3” was not available for download
275 from ESGF, so r2 was substituted instead. Since more than one EURO-CORDEX RCM is driven by the same
276 ensemble member of the same GCM, we repeat these GCMs when calculating the CMIP5 ensemble mean for the
277 common subset. For the CMIP5 vs CORDEX analysis we first bias adjust models before plotting return period
278 curves in order to allow the shapes of the distributions to be compared more easily. We do this by subtracting the
279 difference between the model climatology of the index in question and the climatology of the observations for each
280 model at a grid cell level. We use E-OBS as the reference for temperature and precipitation, and MESCAN for wind.
281 For the UPSCALE simulations, since the same version of the same model is used across each resolution, results can
282 also be examined without bias adjusting the extremes climatology, and this provides some interesting insights.

283

284 Confidence intervals for observations are calculated using a bootstrapping method. If, for example, the analysis
285 period was 1970-2005 (i.e. 36 years), 1000 random samples of 36 years from this period are chosen from the same
286 observations, allowing the same year to be chosen more than once per iteration. For each random sample, the chosen
287 values are sorted for each grid cell and a regional average is calculated as above, effectively yielding 1000 return
288 period curves per region. The 5th and 95th percentile of these values are then calculated to give the confidence
289 intervals.

290
291 Finally, for the HadGEM3-A GCM simulations, a circulation analogue technique is used to split any differences in
292 results according to resolution into upscaling (i.e. improved large scale circulation) and downscaling effects. This is
293 described in section 4.3.

294 **4 Results**

295 **4.1 The benefits of regional high resolution: EURO-CORDEX versus CMIP5**

296 **4.1.1 Temperature extremes**

297 Figure 1 shows the spatial patterns of the climatological mean of TXx5day for the period 1970-2005 for E-OBS, and
298 the multi-model means (MMM) of CMIP5, and CORDEX at both resolutions, along with their biases with respect to
299 E-OBS. The same general pattern can be seen in both the observations and the models, with hotter extremes in the
300 south and cooler extremes in the north and over the mountains. At higher resolution the colder warm extremes over
301 the Alps and Carpathians become more distinct. For the “common subset” the pattern of biases relative to E-OBS is
302 similar for each model category with cold biases in the North and West and hot biases in the South-East. However,
303 the hot biases over the mountains reduce with higher resolution since the model topography is higher. The cold bias
304 over Scandinavia is also larger in CORDEX than in CMIP5. Biases using the whole ensemble are very similar as
305 those for the CORDEX subset, although for CMIP5 the hot biases over the south-east, and over mountain ranges are
306 stronger. Findings for TXx are similar, but hotter (not shown).

307
308 To give an idea of the level of consistency of results between models, results for individual models are shown in
309 figure S3. Although the CMIP5 models agree on the general spatial pattern of temperature extremes, their absolute
310 magnitudes vary considerably, although all are too hot over the Alps. There are also substantial differences between
311 results from different RCMs, including those driven by the same GCM. Biases of individual RCMs do not appear
312 systematically smaller than that of their driving GCM. Patterns are very similar for the same GCM-RCM chains at
313 the both 12.5 and 50 km resolutions. Results for different ensemble members of the same GCM or GCM-RCM chain
314 are very consistent, suggesting that the differences between models are not due to internal variability.

315
316 In order to assess the shape of the statistical distribution of temperature extremes, figure 2 (left column) shows return
317 period against magnitude for TXx5day for CMIP5, CORDEX at both resolutions and E-OBS (see Methods). Results
318 are shown for Northern, Central and Southern Europe, and are representative of the subregions. There is no obvious

319 difference in the shape of the tails between CMIP5 and CORDEX. Agreement with E-OBS is good for the multi
320 model median, although many individual ensemble members lie outside the range of the observational uncertainty,
321 particularly on the heavy tailed side.

322
323 In summary, temperature extremes appear to be relatively insensitive to dynamical downscaling based on comparing
324 CMIP5 to CORDEX at 0.11° and 0.44°, except over mountains where hot biases decrease with resolution.

325 **4.1.2 Precipitation extremes**

326 Now we consider precipitation extremes for CMIP5 compared to CORDEX. Figure 3 shows the climatological mean
327 of Rx1day for E-OBS and the MMMs of CMIP5 and CORDEX at both resolutions, and their differences with
328 respect to E-OBS. The heaviest annual maximum precipitation totals in E-OBS occur over the Alps and the western
329 side of coastal mountain ranges, including western Norway and north-eastern Spain. A similar spatial pattern of
330 precipitation distribution can be seen in the models, although totals are lower in CMIP5, and higher in CORDEX.
331 CMIP5 is drier than E-OBS over most of Europe, particularly over the areas of maximum observed precipitation (i.e.
332 over or near mountains), whilst CORDEX is generally wetter than observed, particularly in these same locations, and
333 at higher resolution. Results using the entire ensembles are very similar to using the common subset of simulations.
334 Previous studies suggest that E-OBS underestimates precipitation extremes since it is not corrected for gauge
335 undercatch and has a relatively low underlying station density (e.g. Prein and Gobiet 2017). Therefore, we also
336 repeat results relative to the MESAN reanalysis (Figure S4) for the shorter period 1989-2005. MESAN uses a
337 particularly high density of stations in France (see Data section). The climatology of Rx1day is wetter in MESAN
338 than in E-OBS over most of Europe, most noticeably over the Alps and surrounding areas. This leads to the dry bias
339 in CMIP5 appearing bigger, and the wet bias in CORDEX decreasing, although it is still present in the 0.11°
340 simulations. Using regional-scale very high resolution datasets could improve agreement with the 0.11° simulations,
341 since they tend to give heavier precipitation extremes (Prein and Gobiet 2017). Gauge undercatch will also contribute
342 to the difference, particularly for precipitation extremes associated with strong winds and in snow dominated regions
343

344 Figure S5 shows results for individual models. Again, whilst models agree on the general pattern of precipitation
345 extremes – i.e. wettest over mountains, there are considerable inter-model differences concerning the magnitude,
346 particularly over complex orography. A number of CMIP5 models have too light extremes everywhere, but all
347 underestimate precipitation extremes over mountainous regions to a greater or lesser extent. RCMs systematically
348 simulate heavier precipitation extremes compared to their driving GCMs, particularly over mountains, and these
349 extremes tend to become heavier when moving from 0.44° to 0.11° in most cases. Many of the RCMs have heavier
350 precipitation extremes than seen in E-Obs over much of Europe at 0.44°, although this difference may disappear if
351 compared to MESAN. This difference gets bigger at higher resolution and is largest over mountainous regions.
352 Again results are very consistent between ensemble members of the same models.

353

354 Figure 2 (middle column) shows return period curves for Rx1day for Northern, Central and Southern Europe. There
355 is a clear separation in the tails of the distribution according to resolution, with CMIP5 having the lightest tails,
356 CORDEX 0.44 in the middle, and CORDEX 0.11 with the heaviest tails across all regions (including the subregions
357 – not shown). Results using the common subset of models or the full ensembles are similar to each other. EObs
358 tends to lie between CMIP5 and CORDEX 0.44 for central and southern Europe, and closer to CORDEX 0.44 in
359 northern Europe. Using MESAN gives slightly heavier tails in central Europe (figure S6) (particularly in France,
360 where station density is highest –not shown) and more so in southern Europe, causing the best agreement to occur
361 with CORDEX 0.44 everywhere. Results for Rx5day are similar, but with marginally less separation between the
362 resolutions, whilst over Northern and Central Europe the best agreement with E-OBS happens at a slightly higher
363 resolution than for Rx1day – i.e. either with CORDEX 0.44 or the lower end of the range of CORDEX 0.11 (not
364 shown).

365
366 In summary, precipitation extremes are wetter and heavier tailed with higher resolution, especially over mountainous
367 regions. CMIP5 has a dry bias, particularly over mountains, whilst CORDEX tends to be too wet relative to E-Obs ,
368 particularly at 0.11°, but results are sensitive to observational dataset used, with wet biases for CORDEX reducing
369 when compared to the higher resolution MESAN dataset.

370 **4.1.3 Wind Extremes**

371 Finally, we examine annual maximum wind (WindXx). Figure 4 shows the multi model means of climatological
372 mean annual maximum wind for CMIP5 and CORDEX at 0.44° and 0.11° compared to three reanalysis datasets.
373 Note however that the model results are based on the annual maximum of the daily maximum surface wind (variable
374 “sfcWindmax”), whilst the reanalysis estimates are based on the annual maximum of 6-hourly data. As a sensitivity
375 test, for CMIP5 models that had both sfcWindmax and 3-hourly data, we compared results using sfcWindmax, 3-
376 hourly and 6-hourly data (Figure S7). 6-hourly data tends to give lower values than using 3-hourly data or
377 sfcWindmax since some events will be missed due to the lower sampling frequency. SfcWindmax appears to be
378 mostly based on the model timestep, and gives higher wind speeds than using 3 or 6 hourly data, with some
379 exceptions, e.g. the IPSL models and CMCC-CM where it gives lower values. This apparent difference in definition
380 between models is a weakness of this analysis. Furthermore, since different models have different time steps, and the
381 time step generally decreases with increased resolution, we might expect stronger winds with increased resolution
382 purely due to the difference in sampling frequency. Whilst it could be argued that this makes the models not strictly
383 comparable, being able to generate stronger winds due to a shorter time step could nevertheless be considered an
384 inherent feature of higher resolution models. It would have been cleaner to use a metric that is more consistent across
385 models, such as 3 hourly or 6 hourly wind speeds. However, CORDEX at 0.44° does not have this data available,
386 whilst CORDEX at 0.11° only has it for a small number of simulations, all of which are based on RCA, and only 3 of
387 which have data for the driving GCM. Therefore, the reader is invited to interpret results with this caveat in mind.
388 Model sfcWindmax estimates may also differ in terms of the treatment of surface roughness length and the method
389 for calculating wind at 10m from wind at a higher level.

390
391 Examining figure 4, the MESCAN and DYNAD reanalyses show strong extreme winds over the UK, the Norwegian
392 mountains and the NW coastline of France through to Denmark. Relatively strong winds are also seen over the
393 Spanish plateau, and a belt of strong winds running zonally across central Europe between slower winds to the North
394 and South. The datasets differ in the magnitude of the winds, with MESCAN having more contrast between areas of
395 low and high wind. ERA5 has notably slower winds, particularly over mountainous regions, but a similar overall
396 zonal tripole pattern can be seen.

397
398 The CMIP5 driving model mean shows a similar overall pattern of WindXx as the reanalyses, with a pattern of
399 weaker winds in the north and south, and a belt of stronger winds in the middle, but do not tend to have stronger
400 winds over mountains like in DYNAD and MESCAN . Using the whole CMIP5 ensemble gives slightly stronger
401 extreme winds. Absolute magnitudes are not directly comparable to the reanalysis estimates, which would be
402 expected to have slightly slower winds due to differences in sampling frequency. The CORDEX multi model means
403 show generally higher wind speeds than CMIP5, and capture the high wind speeds along western coastlines and over
404 mountainous terrain. Differences between the 0.11° and 0.44° runs appear small. Results for the common subset of
405 simulations are very similar to those obtained from the complete CORDEX ensembles. Biases are not shown due to
406 the difference in temporal resolution with respect to the reanalyses.

407
408 Figure S8 shows that there is a large variety between different models, particularly for CMIP5, but also according to
409 RCM. CanESM2 and IPSL-CM5A-LR are notable outliers, and this may be related to the timestep of the wind data
410 used to calculate sfcWindmax in these models. The zonal tripole pattern can be seen in a number of GCMs, as can
411 stronger winds along western and Mediterranean coastlines, and lower wind speeds over the Alps. Spatial patterns
412 for the RCMs are very RCM specific and relatively insensitive to driving GCM. All RCMs agree on higher winds
413 over the British Isles and weaker winds over northern Europe, but notably the mountainous regions have either low
414 or high wind speeds depending on the model, which must relate to how wind speed is calculated there - it can be
415 imagined that the wind speed in a valley would be somewhat different to that at the top of a mountain. In terms of
416 differences between the two resolutions of CORDEX, some RCMs show increased wind speeds with higher
417 resolution e.g. RACMO, HIRHAM5, and others less so. Again, ensemble members of the same model give similar
418 results.

419
420 Figure 2 (right column) shows the return period plots for WindXx for CMIP5 and both resolutions of CORDEX. All
421 models are shifted to have the same climatology of annual maximum wind for each grid cell, which goes some way
422 to adjusting for differences in sampling frequency, although there is evidence that the shape of the tails is also
423 affected for some models (Figure S7). The results for the common subset of CORDEX runs should at least be more
424 directly comparable to each other, although the sampling frequency should still increase at higher resolution. The
425 British Isles are shown instead of Northern Europe, since they are particularly affected by wind extremes, and for
426 comparison with the results for the UPSCALE simulations, where this region shows distinctive results. The
427 distribution of annual maximum sfcWindmax has heavier tails in CORDEX 0.11 compared to 0.44 which is in turn

428 heavier than CMIP5, regardless of the subset of models used in calculating the multi-model median in almost all
429 regions examined. Exact values are somewhat sensitive to the models included for some sub-regions (not shown).
430 Results based on DYNAD and MESCAN tend to lie in between the two CORDEX resolutions, whilst CMIP5 is
431 closest to ERA5.

432
433 In summary, winds tend to be stronger, with heavier tails at higher resolution, with a large spread between models.
434 Reanalysis datasets give fairly diverse results.

435

436 **4.2 Global high resolution: UPSCALE**

437 We now examine the benefits or otherwise of global high vs. standard resolution simulations for simulating climate
438 extremes. Global high resolution may allow an improved representation of the large scale circulation that cannot be
439 captured by regional models, which may in turn affect the representation of climate extremes. For this we examine
440 the UPSCALE simulations (Mizielinski et al. 2014), which consist of a small ensemble of HadGEM3-A simulations
441 at three different resolutions: 130km (N96), 60km (N216), and 25km (N512) (see Data section).

442 **4.2.1 Temperature extremes**

443 Figure 5 shows the ensemble mean climatological mean of TXx5day for the UPSCALE simulations over the period
444 1985-2011 at all three resolutions, and their biases relative to E-OBS. The same general pattern of hotter extremes in
445 the south and colder in the north and over mountainous regions can be seen at all three resolutions, but temperature
446 extremes are hotter at higher resolution in the south and east, and colder over mountains. The same pattern of biases
447 is seen as for CORDEX and CMIP5 with cold biases in the north and hot in the south-east and over mountains. The
448 mountain biases reduce with higher resolution, as the orography becomes better defined, whilst the hot bias in the SE
449 and SW increases and the northern cold bias improves slightly. A coastal cold bias at low resolution disappears at
450 higher resolution as the model land mask becomes more detailed. Note that the SSTs are prescribed and are the same
451 for all simulations. Results for TXx are similar but hotter (not shown).

452
453 Figure 6 (left column) shows regional return period plots for TXx5day for the UPSCALE simulations. Results are a
454 little less consistent across regions for UPSCALE compared to the CMIP5 vs CORDEX analysis, so we split
455 Northern Europe into the British Isles and Scandinavia, and add the Alps, to better capture regional variations. Since
456 the ensemble means are only based on one model, results are presented without adjusting according to the
457 climatology of TXx5day, although bias adjusted results can be seen in Figure S9 and allow differences in the shapes
458 of the tails to be seen more clearly. TXx5day seems to be somewhat hotter with higher resolution over many regions,
459 although this is not always clear cut. The Alps are a notable exception, where the higher elevations with higher
460 resolution give rise to colder temperature extremes. There are notable biases relative to the observations, with the
461 models being too cold in the north, especially at low resolution, whilst in the south the colder subset of models (N96,
462 the lowest UPSCALE resolution) agree best with the observations. Over the Alps, again the low resolution

463 simulations agree best with observations, with the warmest temperatures, but this will depend on the height of the
464 meteorological stations. This apparent contradiction to the reduced orographic hot bias with resolution in figure 5
465 comes from the stronger cold bias of the surrounding areas at low resolution. Figure S9 shows that differences
466 between the shape of the tails with resolution are not systematic across regions and are mostly small. Agreement with
467 E-OBS is good everywhere. Results for TXx are similar.

468
469 In summary, hot biases of temperature extremes over mountains reduce with increased resolution for HadGEM3-A.
470 Elsewhere extremes tend towards getting hotter with resolution, whilst the shapes of the statistical distributions are
471 insensitive.

472 **4.2.2 Precipitation extremes**

473 For precipitation, Figure 7 shows the ensemble mean climatological mean of Rx1day for the period 1989-2010 for
474 the three UPSCALE ensembles and their differences relative to E-OBS and MESAN. The overall pattern of Rx1day
475 is similar to that in E-OBS, with heavier precipitation extremes and finer spatial detail with increasing resolution over
476 complex orography. All resolutions have bands of heavy precipitation either side of the Alps, but these move closer
477 together as the Alps become better defined. All simulations are generally wetter than E-OBS across most of Europe,
478 whilst the dry bias over orography in the Alps, Southern Norway and Scottish Highlands reduces with resolution and
479 a wet bias on the southern edge of the Alps and the coastal side of the Dinaric Alps in the Balkans appears as
480 resolution increases. Comparing to MESAN instead of E-OBS, the general wet bias disappears, and the dry mountain
481 bias over orography at low resolution increases. The differences between resolutions appear smaller than for the
482 CMIP5 versus CORDEX analysis: all the UPSCALE simulations look most similar to CORDEX at 0.44°. However,
483 UPSCALE does not reach as fine a resolution as CORDEX at 0.11° (25 km vs 12.5 km), and CMIP5 is on average
484 slightly coarser than the N96 simulations. In addition, it should be noted that models with the same nominal
485 resolution do not necessarily have the same effective resolution, and that the effective resolution is always less than
486 the nominal resolution (Skamarock 2004; Klavar et al. 2020). Results are similar for Rx5day (not shown).

487
488 Figure 6 (middle column) shows the return period plots for Rx1day for the three resolutions of UPSCALE
489 ensembles. Slightly heavier precipitation extremes are found at higher resolution in all the regions shown (exceptions
490 are France and Mid Europe- not shown), although differences are small, they are more obvious in southern Europe
491 and especially in the Alps. Figure S9 shows that there is not much difference in the shape of the tails for most
492 regions, although there are very slightly heavier tails at higher resolution for southern Europe (more so in the
493 Mediterranean sub region- not shown) and more obvious differences over the Alps in the same direction, both of
494 which are regions where convective precipitation is important. E-OBS tends to lie just below the model simulations
495 for most regions (Figure 6), although it agrees with the models for the British Isles, and is between the low and
496 medium resolution simulations over the Alps. MESAN gives higher values for observed Rx1day which improves
497 agreement in regions where E-OBS lay below the models, and causes a higher resolution subset to agree better in the
498 other regions (Figure 6). For the bias adjusted curves E-OBS tends to lie just on the lower end of the ensemble for

499 most regions, whilst MESAN gives slightly heavier tails and tends to improve agreement with models (Figure S9).
500 Results for Rx5day are broadly similar (except that both sets of observations lie above all the models for the British
501 Isles).

502
503 In summary, precipitation extremes are somewhat wetter and heavier tailed with increasing resolution mostly in
504 southern Europe and the Alps for HadGEM3-A. Dry orographic biases decrease with resolution, but wet biases
505 appear in the south next to mountain ranges instead.

506 **4.2.3 Wind extremes**

507 For wind extremes, Figure 8 shows the spatial patterns of climatological mean annual maximum wind based on 6-
508 hourly data for UPSCALE and the same for three reanalyses. In this case the models and reanalyses are directly
509 comparable since they share the same temporal resolution. The spatial patterns are similar for the three different
510 model resolutions, with the highest winds over the British Isles and coastal regions, lower wind speeds over the Alps,
511 and the zonal tripole pattern described above. The main differences are that the lower resolution model (N96) has
512 stronger winds around the British Isles and western coastlines. This is likely because the larger coastal grid boxes
513 overlap more with the ocean, which tends to have higher wind speeds, or due to differences in the model land mask
514 itself with resolution. The wind speeds at higher resolution are a little stronger overall, most obviously in the central
515 European zonal belt, and over the Alps and Norwegian mountains. All resolutions show stronger winds than ERA5
516 over most of Europe. Compared to MESCAN winds are too weak in the northern and southern Europe, particularly
517 over mountainous regions, and a little too strong in between. Relative to DYNAD the pattern of differences is similar
518 as for MESCAN, but with stronger negative differences over the Norwegian mountains and positive differences in
519 other parts of Northern Europe. There are positive coastal biases relative to all reanalyses that reduce with increased
520 resolution.

521
522 Figure 6 (right column) shows the return period plots for some example regions for annual maximum wind for the
523 UPSCALE simulations, without shifting the climatology. Over all regions examined (except the Mediterranean- not
524 shown), the N512 simulations have stronger winds than the N216 simulations. The position of the curve for N96 is
525 strongly related to how much coastline there is relative to land area per region, e.g. with faster winds than the other
526 simulations over the British Isles and southern Europe, but relatively slower winds over central Europe, and
527 particularly over the Alps (not shown). There are fairly large differences between reanalysis estimates, with ERA5
528 always having the slowest winds, and the model simulations tending to lie between ERA5 and the other two
529 reanalyses for most regions. For the bias adjusted versions of the return period plots (Figure S9), differences in the
530 shapes of the tails with resolution are generally small, although with marginally heavier tails with increasing
531 resolution over a number of regions (not all are shown). The shape of the tails is generally close to the reanalysis
532 estimates.

533

534 In summary winds are slightly stronger and heavier tailed at higher resolution in HadGEM3-A, except over coastal
535 areas where large coastal grid boxes at low resolution bring strong ocean winds further over land.

536 **4.3 Circulation Analogues**

537 For the global model results, any differences in the representation of extremes according to resolution could come
538 from either upscaling or downscaling effects. Upscaling effects could include a better representation of the large
539 scale circulation, whilst downscaling allows a better representation of small scale processes, such as convection, and
540 an improved representation of orography and coastlines. In order to investigate which of these effects leads to the
541 differences between the low (N96) and high resolution (N512) HadGEM3-A simulations, we employ a circulation
542 analogue technique (e.g. Vautard et al., 2016), which is frequently used in attribution studies (see e.g. Stott et al.,
543 2016; Cattiaux et al., 2010). The idea is to determine whether the simulation of climate extremes changes between
544 the two resolutions if both were to have the same large scale circulation –i.e. isolating the downscaling effect, or
545 conversely whether circulation differences explain any differences in extreme events whilst circulation-variable (e.g.
546 precipitation) relationships stay the same –i.e. the upscaling effect.

547
548 For each day in the lower resolution simulations we pick the nearest circulation analogue from anywhere in the
549 higher resolution simulations, providing it happens at the right time of year (i.e. within a 30-day window centred on
550 the day of the year in question). We then record the associated temperature, precipitation and wind values from the
551 higher resolution simulations to make a “*u*-chronic” dataset (e.g. Jézéquel, et al. 2018) that contains data from the
552 high resolution simulations but follows the daily sequence of circulation patterns from the low resolution models. We
553 then repeat the analysis of return periods and value as above. We also do the reverse (find analogues for the N512
554 circulation in the N96 ensemble and record the N96 temperature). Since results using analogues are not directly
555 comparable to the original results, due to lack of exact analogue match, we also perform “self-analogues” -i.e.
556 finding circulation analogues for the N96 simulations within the N96 ensemble, (excluding the same year from the
557 same ensemble member) and creating a *u*-chronic time series, and the same for the N512 ensemble). Comparing the
558 resulting return period curves tells us about the contribution of large-scale circulation and downscaling to differences
559 in extremes between the two resolutions. For example, comparing the N96 self-analogue return curve to the version
560 based on N512 circulation but with N96 precipitation shows us the contribution of any differences in the large scale
561 circulation between the resolutions i.e. the upscaling effect. Comparing the N96 self-analogue to the version based
562 on N96 circulation with N512 precipitation shows us the downscaling effect – i.e. any difference between the
563 relationship between the large scale circulation and precipitation.

564
565 Analogues are defined using geopotential height at 500 hPa, since this avoids complications relating to surface heat
566 lows associated with heat waves in anticyclonic conditions that occur in summer, whilst also avoiding incomplete
567 data due to mountain ranges. Geopotential height is regridded to a 2° grid using bilinear interpolation. This choice
568 ensures that we are comparing analogues with the same resolution and do not penalise small-scale differences.
569 Similarity between circulation states is quantified using pattern correlation, which is not affected by trends in

570 geopotential height with global warming. For precipitation and wind the European domain used is -16 to 44° E and
571 34 to 72° N (roughly the same as the domain plotted in the map-based figures). For temperature, a larger domain is
572 used, since the history and trajectory of air masses are important for temperature extremes. This domain is loosely
573 based on the domain used by Cattiaux et al. (2010) and extends over the N. Atlantic as well as Europe, (-62 to 44°E
574 and 24 to 80° N). However, results are very similar if the smaller domain is used (not shown). For the 5-day
575 variables (Rx5day and TXx5day); daily geopotential height, precipitation and temperature datasets were smoothed
576 using a 5-day running mean first, and then analogues were calculated, and the u-chronic datasets constructed. We
577 also tried doing the 5-day means last rather than first, i.e. calculating analogues using daily data and smoothing the u-
578 chronic dataset. The relationship between the different curves was largely consistent between the two techniques, but
579 absolute values differed and the shape of the distributions changed a little. Results presented here are based on the
580 first technique since it replicates better the autocorrelation structure of the original analysis.

581
582 Figure 9 shows the results of the analogue analysis. The blue curves show the results for the N512 self-analogues,
583 grey represents the N96 self-analogues, red represents results using the circulation patterns from the N96 runs but
584 with the N512 circulation-variable relationships, and green indicates N512 circulation with N96 circulation-variable
585 relationships. The difference between the blue and red curves (or the grey and green curves) shows the contribution
586 from differences in the large scale circulation with resolution, whilst the difference between the blue and green
587 curves (or the red and grey curves) indicates the downscaling effect.

588
589 For TXx5day downscaling effects are dominant over regions that have a clear difference between resolutions,
590 although circulation differences also have a small effect in some regions such as the British Isles (Figure 9). For
591 Rx1day the different curves are very close together for most regions, making it difficult to discern the relative
592 contributions from upscaling and downscaling. However, it generally seems to be downscaling effects that are the
593 most important, and this can be seen more clearly for the Alps and Southern Europe where there are larger
594 differences with resolution. Interestingly, these are regions where convective precipitation is particularly important
595 for precipitation extremes. For wind extremes downscaling effects also dominate. Results for TXx and Rx5day are
596 very similar to those for TXx5day and Rx1day respectively (not shown).

597
598 Also shown, using dashed lines, are the original ensemble mean results without using analogues. By comparing these
599 with the self-analogue results we can see how successful the analogue technique is in recreating the original
600 distributions. The self-analogue results tend to be close to the original results for wind and Rx1day, but above them
601 for Tx5day. This effect seems to be enhanced by the 5 day averaging, but is still present for TXx (not shown).
602 Undertaking the 5-day averaging last rather than first (see Methods) shifts analogue results downwards, underneath
603 the original curves, but otherwise gives the same results (not shown). A similar phenomenon is seen for Rx5day (not
604 shown).

605

606 In summary, for all three types of extreme events, downscaling effects appear to dominate the differences seen
607 between the 130km and 25km HadGEM3-A simulations. This suggests that at least for this model, any large scale
608 circulation differences obtained with global high resolution do not affect the statistics of these extreme events much.

609 **5 Discussion and Conclusions**

610 We evaluated climate model simulations of temperature, precipitation and wind extremes over Europe, addressing
611 three questions: 1) The benefits of dynamical downscaling using regional climate models by comparing EURO-
612 CORDEX simulations at two resolutions (12.5 and 50 km) to their driving coarser resolution CMIP5 models; 2) The
613 benefits of increased resolution for global models by comparing HadGEM3-A simulations at three resolutions (130,
614 60 and 25 km; referred to as the “UPSCALE” simulations); and 3) whether any differences according to resolution in
615 the global model comes from differences in the large scale circulation (upscaling) or the representation of small scale
616 processes, and features (downscaling) using a circulation analogue method.

617
618 For temperature extremes, increased resolution did not make much difference to results for the CORDEX vs CMIP5
619 analysis, both in terms of the shapes of the distributions, which all agreed well with observations, or in terms of
620 biases, apart from reducing hot biases over mountains. These findings agree with Vautard et al. (2013), who find
621 limited benefits in simulating various aspects of heatwaves between the 0.44° and 0.11° versions of the EURO-
622 CORDEX models. This reduction in orographic bias with increased resolution was also seen in the HadGEM3-A
623 GCM simulations, along with a general tendency towards hotter extremes elsewhere, which reduces biases in the
624 north, and increases them in the south. Overall the benefits of increasing resolution were limited, or region
625 dependent. However, our results for the global model analysis are based on only one model and the new model
626 simulations and analyses being generated as part of the PRIMAVERA and HighResMIP projects
627 (<https://www.primavera-h2020.eu/>; Roberts et al. 2018; Haarsma et al. 2016) will be very useful for determining how
628 representative our results for HadGEM3-A are of other GCMs. For instance, improvements in the simulation of
629 summer blocking, which can be involved in heatwave generation is very model dependent (Scheimann et al. 2014).
630 Furthermore, Cattiaux et al. (2013) find that the frequency, intensity and duration of summer heatwaves improve in
631 the IPSL model with resolution, associated with a better representation of the large scale circulation. In addition, here
632 we examine only one aspect of heat waves (intensity), and it could be that results are different for other aspects, such
633 as frequency, duration and timing.

634
635 Precipitation extremes were more sensitive to resolution, particularly in the CMIP5 vs CORDEX analysis, with
636 heavier tails at higher resolution across all regions. Spatially, CMIP5 shows a general dry bias compared to E-OBS,
637 particularly over mountainous regions, whilst CORDEX shows the opposite, with increasing wet differences at 0.11°
638 compared to 0.44°, which appears to be systematic across models. This is consistent with results for mean
639 precipitation in EURO-CORDEX in Kotlarski et al. (2014). The higher resolution MESAN reanalysis gave wetter
640 extremes and heavier tails than E-OBS, agreeing best with the 0.44° resolution CORDEX simulations. Other studies
641 suggest that country-scale higher resolution precipitation datasets give heavier precipitation extremes still, which

642 may agree best with the 0.11° simulations. Similarly, for mean precipitation, Prein and Gobeit (2017) find that RCM
643 biases are a similar size to the differences between different observational estimates. For extreme precipitation, Prein
644 et al (2016) and Torma et al (2015) find that various aspects (biases, frequency-intensity distributions, spatial
645 patterns) of mean and extreme precipitation improve in EURO-CORDEX at 0.11° compared to 0.44° when
646 compared to such datasets for Europe and the Alps respectively. Prein et al (2016) ascribe this mostly to the better
647 representation of orography at higher resolution, but also the ability to capture the larger scales of convection.
648 However, aside from improved spatial patterns Casanueva et al (2016) found only limited evidence for
649 improvements in precipitation intensity, frequency and derived indicators over the Alps and Spain with resolution in
650 EURO-CORDEX. Some of the differences with resolution in our results may also be explained by parameterisation
651 schemes that tend to be tuned to one resolution and can behave sub-optimally at others.

652
653 For the UPSCALE global simulations, there was less difference with resolution, with the biggest differences in
654 southern regions or over or near mountains, with heavier tails and wetter extremes at higher resolution. This reduced
655 dry biases over orography, but wet biases next to some mountain ranges in the south emerged instead. However, these
656 simulations span a narrower range of resolutions, i.e. not reaching the same high resolutions as CORDEX 0.11° , but
657 also not as coarse as some CMIP5 models. Other global model studies also tend to find an increase in precipitation
658 extremes with increased resolution for Europe, which is continent-wide in summer, and concentrated in mountainous
659 regions in winter (Volosciuk et al. 2015; Wehner et al. 2014). This sometimes improves agreement with observations
660 (e.g. Kopparla et al. 2013; Wehner et al. 2014 for winter), but can overestimate summer extreme precipitation if
661 parameterisation schemes are not retuned (Wehner et al. 2014).

662
663 For wind extremes, higher resolution gave stronger winds and heavier tails for most regions for both the CORDEX
664 vs CMIP5 analysis and to a lesser extent for HadGEM3-A, except for regions dominated by coasts for the latter,
665 where large coastal grid boxes at lower resolution brought strong ocean winds further over land. Stronger winds with
666 higher resolution are also found in previous studies (e.g. Pryor et al. 2012; Kunz et al. 2010). The largest differences
667 we found were between CMIP5 and CORDEX at 0.44° , with less difference between the two resolutions of
668 CORDEX. Differences between reanalysis based estimates made model evaluation difficult, whilst inconsistencies in
669 the way daily maximum wind is calculated in different models were also an issue.

670
671 The results of the circulation analogue analysis on the HadGEM3-A GCM simulations suggested that downscaling
672 effects were the dominant cause of differences with resolution for all three phenomena, with limited effects of any
673 differences in the representation of the large scale circulation. If this result also applied to other GCMs, it would
674 suggest that dynamical downscaling with more economical limited area models would be a better strategy for
675 simulating European extreme events, whilst GCM efforts could focus on other aspects such as multiple members or
676 multi-physics ensembles. However, we cannot reach this conclusion based solely on this analysis, since we examine
677 only a single model, which may not be representative of other models, and because the range of resolutions
678 considered may be too narrow. Furthermore, a number of studies do find improvements in the large-scale circulation
679 with resolution, including for extra-tropical cyclones and storm tracks (Colle et al. 2013; Jung et al 2006; 2012,

680 Zappa et al. 2013), Euro-Atlantic weather regimes (Dawson et al. 2012; 2015; Cattiaux et al. 2013) and blocking
681 (Jung et al. 2012, Anstey et al. 2013; Matsueda et al. 2009, Berckmans et al 2013; Scheimann et al. 2014; Davini et
682 al 2017a; 2017b; see also Introduction). Interestingly, Scheimann et al. (2017) find improvements in Euro-Atlantic
683 blocking with resolution in all seasons in the same HadGEM3-A simulations as we analyse here. However, the net
684 effects on extremes, given all uncertainties, was not explicitly investigated. Our study does not seem to be able to
685 discern such effects. Other studies suggest that benefits from upscaling may require convective permitting
686 simulations (Hart et al. 2018).

687
688 Overall our results suggest that whether or not increased resolution is beneficial for the simulation of extreme events
689 over Europe depends on the event being considered. Benefits appear limited for heatwaves, whereas wind extremes
690 and particularly precipitation extremes are more sensitive. We do not find any particular advantage in using a global
691 high resolution model compared to regional dynamical downscaling, with the caveats that this investigation needs to
692 be extended to other GCMs, and a wider range of resolutions should be investigated.

693
694 In order to fully address the question of the benefits of increased resolution for European climate extremes, a number
695 of aspects remain to be investigated. Firstly, the analysis could be widened to other types of extremes, for example,
696 sea level rise and storm surge, or other aspects of extremes could be considered e.g. timing, frequency and duration
697 of events. The global simulations we investigated were atmosphere-only, and the role of increased ocean resolution
698 and also vertical resolution and model top height should be considered. Finally, we assume that better historical
699 performance translates into more accurate future projections. Lhotka et al. (2018) find low sensitivity of heatwave
700 projections to resolution in EURO-CORDEX RCMs. However, Van Haren et al. (2015b) find stronger future
701 summer drying and heating in central Europe with increased resolution in the EC-Earth GCM due to differences in
702 atmospheric circulation. Concerning precipitation, future projections for large scale and seasonal mean precipitation
703 are consistent between large scale regional and convective permitting models, whilst there is evidence that summer
704 sub-daily intensities increase more in the future in convection permitting models (Kendon et al. 2014; 2017; Ban et
705 al. 2015). For wind, Willison et al. (2015) find a larger response of the North Atlantic storm track to global warming
706 with higher resolution in the regional WRF model. Furthermore, Baker et al. (2019) find that in winter the polar jet,
707 storm tracks and associated precipitation shift further North over the Euro-Atlantic region the future with increased
708 resolution in the same HadGEM3-A set up as used here. The sensitivity of projections to resolution nevertheless
709 remains an area that needs further research.

710 **Data and code availability**

711 The CMIP5 and CORDEX data used for this analysis are available from the Earth System Grid Federation portals,
712 and are detailed in Table S1. The HadGEM3-A UPSCALE simulations are available from the CEDA-JASMIN
713 platform. E-OBS can be downloaded here <https://www.ecad.eu/download/ensembles/download.php>, MESAN is
714 available here <http://exporter.nsc.liu.se/620eed0cb2c74c859f7d6db81742e114/>, ERA5 and MESCAN are available

715 from the Copernicus Climate Data Store <https://cds.climate.copernicus.eu>, whilst DYNAD winds are available from
716 Tomas Landelius at SMHI.

717 **Author contributions**

718 CI, RV and SJ conceptualised the study, CI carried out the analysis and wrote the manuscript, JS managed the
719 CRECP project together with CH and BE, and all co-authors were involved in discussions to prepare the study and
720 helped improve the manuscript.

721 **Competing interests**

722 The authors declare that they have no conflict of interest.

723 **Acknowledgements**

724 This work is published in the name of the European Commission, with funding from the European Union through the
725 Copernicus Climate Change Service project C3S_34a Lot 3 (Copernicus Roadmap for European Climate
726 Projections). The Commission is not responsible for any use that may be made of the information contained. We
727 acknowledge the WCRP's Working Group on Regional Climate, and the Working Group on Coupled Modelling - the
728 coordinating body of CORDEX and the panel responsible for CMIP5 respectively. We thank the climate modelling
729 groups for producing and making available the model output listed in Supplementary Table 1, which is available at
730 <http://pcmdi9.llnl.gov>. For CMIP, the US Department of Energy's Program for Climate Model Diagnosis and
731 Intercomparison provides coordinating support and led development of software infrastructure in partnership with
732 the Global Organization for Earth System Science Portals. We thank the modelling team that produced the
733 UPSCALE simulations, and acknowledge the JASMIN and IPSL mesocentre computing clusters on which this
734 analysis was performed. We thank Tomas Landelius from SMHI for making the DYNAD wind data available. We
735 also acknowledge helpful input from the CRECP project scientific advisory board and useful discussions with UK
736 Met Office Scientists, in particular Malcolm Roberts and Carol McSweeney.
737

738 **References**

739 Anstey, J. A., Davini, P., Gray, L. J., Woollings, T. J., Butchart, N., Cagnazzo, C., Christiansen, B., Hardiman, S. C.,
740 Osprey, S. M. and Yang, S.: Multi-model analysis of Northern Hemisphere winter blocking: Model biases and the
741 role of resolution, *J. Geophys. Res. Atmos.*, 118, 3956–3971, doi: 10.1002/jgrd.50231, 2013.
742
743 Baker, A.J., Schiemann, R., Hodges, K. I., Demory, M., Mizielinski, M. S., Roberts, M. J., Shaffrey, L. C., Strachan,
744 J. and Vidale, P. L.: Enhanced Climate Change Response of Wintertime North Atlantic Circulation, Cyclonic

745 Activity, and Precipitation in a 25-km-Resolution Global Atmospheric Model. *J. Climate*, 32, 7763–
746 7781, <https://doi-org.ezproxy.is.ed.ac.uk/10.1175/JCLI-D-19-0054.1>, 2019
747

748 Ban, N., Schmidli, J. and Schär, C.: Heavy precipitation in a changing climate: Does short-term summer precipitation
749 increase faster?, *Geophys. Res. Lett.*, 42, 1165–1172, doi: 10.1002/2014GL062588, 2015.
750

751 Bazile, E., Abida, R., Verrelle, A., Le Moigne, P. and Szczypta, C. : Report for the 55years MESCAN-SURFEX re-
752 analysis, deliverable D2.8of the UERRA project, pp. 22, available from:
753 <http://www.uerra.eu/publications/deliverable-reports.html>, 2017
754

755 Berckmans, J., Woollings, T., Demory, M. E., Vidale, P.-L. and Roberts, M.: Atmospheric blocking in a high
756 resolution climate model: influences of mean state, orography and eddy forcing, *Atmos. Sci. Lett.*, 14, 34–40,
757 doi:10.1002/asl2.412, 2013.
758

759 Casanueva, A., Kotlarski, S., Herrera, S., Fernández, J., Gutiérrez, J.M., Boberg, F., Colette, A., Christensen, O. B.,
760 Goergen, K., Jacob, D., Keuler, K., Nikulin, G., Teichmann C. and Vautard, R.: Daily precipitation statistics in a
761 EURO-CORDEX RCM ensemble: added value of raw and bias-corrected high-resolution simulations, *Clim Dynam.*,
762 47,719-737. <https://doi.org/10.1007/s00382-015-2865-x>, 2016
763

764 Cattiaux, J., Vautard, R., Cassou, C., Yiou, P., Masson-Delmotte, V., and Codron, F.: Winter 2010 in Europe: A cold
765 extreme in a warming climate, *Geophys. Res. Lett.*, 37, L20704, doi: 10.1029/2010GL044613, 2010.
766

767 Cattiaux, J., Quesada, B., Arakélian, A., Codron, F., Vautard, R., Yiou, P.: North-Atlantic dynamics and European
768 temperature extremes in the IPSL model: sensitivity to atmospheric resolution, *Clim. Dynam.*, 40, 2293-2310,
769 doi:10.1007/s00382-012-1529-3, 2013.
770

771 Christensen, J. H. and Christensen, O. B.: A summary of the PRUDENCE model projections of changes in European
772 climate by the end of this century, *Climatic Change*, 81, 7–30, doi: 10.1007/s10584-006-9210-7, 2007.
773

774 Colle, B. A., Zhang, Z., Lombardo, K., Liu, P., Chang, E. and Zhang, M.: Historical evaluation and future prediction
775 in Eastern North America and western Atlantic extratropical cyclones in the CMIP5 models during the cool season,
776 *J. Climate.*, 26, 882–903, doi: 10.1175/JCLI-D-12-00498.1, 2013.
777

778 Coppola, E., Sobolowski, S., Pichelli, E., Raffaele, F., Ahrens, B., Anders, I., Ban, N., Bastin, S., Belda, M., Belusic,
779 D., Caldas-Alvarez, A., Margarida Cardos, R., Davolio, S., Dobler, A., Fernandez, J., Fita Borrell, L., Fumiere, Q.,
780 Giorgi, F., Goergen, K., Guettler, I., Halenka, T., Heinzeller, D., Hodnebrog, Ø., Jacob, D., Kartsios, S., Katragko,
781 E., Kendon, E., Khodayar, S., Kunstmann, H., Knist, S., Lavín, A., Lind, P., Lorenz, T., Maraun, D., Marelle, L., van

782 Meijgaard, E., Milovac, J., Myhre, G., Panitz, H.-J., Piazza, M., Raffa, M., Raub, T., Rockel, B., Schär, C., Sieck, K.,
783 Soares, P. M. M., Somot, S., Srnec, L., Stocchi, P., Tölle, M., Truhetz, H., Vautard, R., de Vries, H. and Warrach-
784 Sagi, K.: A first-of-its-kind multi-model convection permitting ensemble for investigating convective phenomena
785 over Europe and the Mediterranean, *Clim. Dynam.*, 1-32, <https://doi.org/10.1007/s00382-018-4521-8>, 2018.

786

787 Dahlgren, P., Landelius, T., Kållberg, P. and Gollvik, S., A high-resolution regional reanalysis for Europe. Part 1:
788 Three-dimensional reanalysis with the regional High-Resolution Limited-Area Model (HIRLAM), *Q.J.R. Meteorol.*
789 *Soc.*, 142, 2119-2131, doi:10.1002/qj.2807, 2016

790

791 Davini, P., Corti, S., D'Andrea, F., Rivière, G., and von Hardenberg, J.: Improved Winter European Atmospheric
792 Blocking Frequencies in High-Resolution Global Climate Simulations. *J. Adv. Model. Earth Syst.*, 9, 2615–2634,
793 <https://doi.org/10.1002/2017MS001082>, 2017a.

794

795 Davini, P., von Hardenberg, J., Corti, S., Christensen, H. M., Juricke, S., Subramanian, A., Watson, P. A. G.,
796 Weisheimer, A., and Palmer, T. N.: Climate SPHINX: evaluating the impact of resolution and stochastic physics
797 parameterisations in the EC-Earth global climate model, *Geosci. Model Dev.*, 10, 1383-1402,
798 <https://doi.org/10.5194/gmd-10-1383-2017>, 2017b.

799

800 Dawson, A. and Palmer, T. N.: Simulating weather regimes: impact of model resolution and stochastic
801 parameterization. *Clim Dynam*, 44, 2177-2193, <https://doi.org/10.1007/s00382-014-2238-x>, 2015.

802

803 Dawson, A., Palmer, T. N., and Corti, S.: Simulating regime structures in weather and climate prediction models,
804 *Geophys. Res. Lett*, 39, L21805, <https://doi.org/10.1029/2012GL053284>, 2012.

805

806 Dee, D. P., Uppala, S. M., Simmons, A. J, Berrisford, P., Poli, P., Kobayashi, S., Andrae, U., Balmaseda, M. A.,
807 Balsamo, G., Bauer, P., Bechtold, P., Beljaars, A. C., van de Berg, L., Bidlot, J., Bormann, N., Delsol, C., Dragani,
808 R., Fuentes, M., Geer, A. J., Haimberger, L., Healy, S. B., Hersbach, H., Hólm, E. V., Isaksen, L., Kållberg, P.,
809 Köhler, M., Matricardi, M., McNally, A. P., Monge-Sanz, B. M., Morcrette, J., Park, B., Peubey, C., de Rosnay, P.,
810 Tavolato, C., Thépaut, J. and Vitart, F.: The ERA-Interim reanalysis: Configuration and performance of the data
811 assimilation system, *Q. J. R. Meteorol. Soc.*, 137, 553–597, <https://doi.org/10.1002/qj.828>, 2011.

812

813 Demory, M. E., Vidale, P. L., Roberts, M. J., Berrisford, P., Strachan, J., Schiemann, R., and Mizielinski, M. S.: The
814 role of horizontal resolution in simulating drivers of the global hydrological cycle, *Clim. Dynam.*, 42, 2201–2225,
815 <https://doi.org/10.1007/s00382-013-1924-4>, 2014.

816

817 Donat M. G., Leckebusch G. C., Wild S., Ulbrich U.: Benefits and limitations of regional multi-model ensembles for
818 storm loss estimations, *Clim. Res.*, 44, 211-225. <https://doi.org/10.3354/cr00891>, 2010.

819

820 Donlon, C. J., Martin, M., Stark, J., Roberts-Jones, J., Fiedler, E., and Wimmer, W.: The Operational Sea Surface
821 Temperature and Sea Ice Analysis (OSTIA) system, *Remote Sens. Environ.*, 116, 140–158,
822 doi:10.1016/j.rse.2010.10.017, 2012.

823

824 Førland, E. and Instituttt, N. M.: Manual for Operational Correction of Nordic Precipitation Data. Norwegian
825 Meteorological Institute., 1996.

826

827 Giorgi F., Jones C., Asrar G. R.: Addressing climate information needs at the regional level: the CORDEX
828 framework, *WMO Bull.*, 58:175–183, 2009.

829

830 Goodison, B. E., Louie, P. Y. and Yang, D.: The WMO solid precipitation measurement intercomparison. World
831 Meteorological Organization-Publications-WMO TD, Report No. 67, 65–70, 1997.

832

833 Gutjahr, O., Schefczyk, L., Reiter, P. and Heinemann, G.: Impact of the horizontal resolution on the simulation of
834 extremes in COSMO-CLM, *Meteorol. Z.*, 25, 543 – 562, doi: 10.1127/metz/2016/0638, 2016.

835

836 Haarsma, R. J., Roberts, M. J., Vidale, P. L., Senior, C. A., Bellucci, A., Bao, Q., Chang, P., Corti, S., Fuckar, N. S.,
837 Guemas, V., von Hardenberg, J., Hazeleger, W., Kodama, C., Koenigk, T., Leung, L. R., Lu, J., Luo, J.-J., Mao, J.,
838 Mizielinski, M. S., Mizuta, R., Nobre, P., Satoh, M., Scoccimarro, E., Semmler, T., Small, J., and von Storch, J.-S.:
839 High Resolution Model Intercomparison Project (HighResMIP v1.0) for CMIP6, *Geosci. Model Dev.*, 9, 4185-4208,
840 <https://doi.org/10.5194/gmd-9-4185-2016>, 2016.

841

842 Hart, N. C. G., Washington, R., and Stratton, R. A.: Stronger local overturning in convective-permitting regional
843 climate model improves simulation of the subtropical annual cycle. *Geophys. Res. Lett.*, 45, 11334–11342,
844 <https://doi.org/10.1029/2018GL079563>, 2018.

845

846 Haylock, M. R., Hofstra, N., Klein Tank, A. M. G., Klok, E. J., Jones, P. D., New, M.: A European daily high-
847 resolution gridded data set of surface temperature and precipitation for 1950-2006. *J. Geophys. Res. Atmos.*, 113,
848 D20119. doi:10.1029/2008JD010201, 2008.

849

850 Hersbach, H., Bell, B., Berrisford, P., Horányi, A., Muñoz-Sabater, J., Nicolas, J., Radu, R., Schepers, D., Simmons,
851 A., Soci, C., Dee, D.: Global reanalysis: goodbye ERA-Interim, hello ERA5. ECMWF, doi:10.21957/vf291hehd7.
852 <https://www.ecmwf.int/node/19027>, 2019

853

854 Herrmann, M., Somot, S., Calmanti, S., Dubois, C., and Sevault, F.: Representation of spatial and temporal
855 variability of daily wind speed and of intense wind events over the Mediterranean Sea using dynamical downscaling:
856 impact of the regional climate model configuration, *Nat. Hazards Earth Syst. Sci.*, 11, 1983-2001,
857 <https://doi.org/10.5194/nhess-11-1983-2011>, 2011.

858
859 Jacob, D., Petersen, J., Eggert, B., Alias, A., Christensen, O. B., Bouwer, L. M., Braun, A., Colette, A., Déqué, M.,
860 Georgievski, G., Georgopoulou, E., Gobiet, A., Menut, L., Nikulin, G., Haensler, A., Hempelmann, N., Jones, C.,
861 Keuler, K., Ko-vats, S., Kröner, N., Kotlarski, S., Kriegsmann, A., Martin, E., Meijgaard, E. van, Moseley, C.,
862 Pfeifer, S., Preuschmann, S., Radermacher, C., Radtke, K., Rechid, D., Rounsevell, M., Samuelsson, P., Somot, S.,
863 Soussana, J.-F., Teichmann, C., Valentini, R., Vautard, R., Weber, B., and Yiou, P.: EURO-CORDEX: new high-
864 resolution climate change projections for European impact research, *Reg. Environ. Change*, 14, 563–578,
865 doi:10.1007/s10113-013-0499-2, 2014.

866
867 Jézéquel, A., Yiou, P. and Radanovics, S.: Role of circulation in European heatwaves using flow analogues. *Clim.*
868 *Dynam.* 50, 1145-1159, <https://doi.org/10.1007/s00382-017-3667-0>, 2018.

869
870 Jung, T., Gulev, S. K., Rudeva, I. and Soloviov, V.: Sensitivity of extratropical cyclone characteristics to horizontal
871 resolution in the ECMWF model. *Q.J.R. Meteorol. Soc.*, 132, 1839-1857, doi:10.1256/qj.05.212, 2006.

872
873 Jung, T., Miller, M. J., Palmer, T. N., Towers, P., Wedi, N., Achuthavarier, D., Adams, J. M., Altshuler, E. L., Cash,
874 B. A., Kinter, J. L., Marx, L., Stan, C., and Hodges, K. I.: High-Resolution Global Climate Simulations with the
875 ECMWF Model in Project Athena: Experimental Design, Model Climate, and Seasonal Forecast Skill, *J. Climate.*,
876 25, 3155–3172, doi:10.1175/JCLI-D-11-00265.1, 2012.

877
878 Kendon, E. J., Roberts, N. M., Senior, C. A., and Roberts, M. J.: Realism of rainfall in a very high-resolution
879 regional climate model, *J. Climate.*, 25, 5791–5806. doi: 10.1175/JCLI-D-11-00562.1, 2012.

880
881 Kendon, E. J., Roberts, N. M., Fowler, H. J., Roberts, M. J., Chan, S. C., and Senior, C. A.: Heavier summer
882 downpours with climate change revealed by weather forecast resolution model, *Nat. Clim. Change*, 4, 570–576, doi:
883 10.1038/nclimate2258, 2014.

884
885 Kendon, E. J., Ban, N., Roberts, N. M., Fowler, H. J., Roberts, M. J., Chan, S. C., Evans, J. P., Fosser, G. and
886 Wilkinson, J.M.: Do Convection-Permitting Regional Climate Models Improve Projections of Future Precipitation
887 Change?. *B. Am. Meteorol. Soc.*, 98, 79–93, <https://doi.org/10.1175/BAMS-D-15-0004.1>, 2017.

888
889 Klaver, R., Haarsma, R., Vidale, P. L., Hazeleger, W.: Effective resolution in high resolution global atmospheric
890 models for climate studies. *Atmos Sci Lett.*, 1– 8. <https://doi.org/10.1002/asl.952>, 2020

891
892 Kopparla, P., Fischer, E. M., Hannay, C., and Knutti, R.: Improved simulation of extreme precipitation in a
893 high-resolution atmosphere model, *Geophys. Res. Lett.*, 40, 5803-5808, doi: 10.1002/2013GL057866, 2013.

894

895 Kunz, M., Mohr, S., Rauthe, M., Lux, R., and Kottmeier, C.: Assessment of extreme wind speeds from Regional
896 Climate Models – Part 1: Estimation of return values and their evaluation, *Nat. Hazards Earth Syst. Sci.*, 10, 907-
897 922, <https://doi.org/10.5194/nhess-10-907-2010>, 2010.
898

899 Landelius, T., Dahlgren, P., Gollvik, S., Jansson, A. and Olsson, E.: A high-resolution regional reanalysis for
900 Europe. Part 2: 2D analysis of surface temperature, precipitation and wind, *Q. J. R. Meteorol. Soc.*, 142, 2132–2142,
901 [doi:10.1002/qj.2813](https://doi.org/10.1002/qj.2813), 2016.
902

903 Lhotka, O., Kyselý, J. and Farda, A.: Climate change scenarios of heat waves in Central Europe and their
904 uncertainties. *Theor Appl Climatol.*, 131, 1043-1054, <https://doi.org/10.1007/s00704-016-2031-3>, 2018.
905

906 Matsueda, M., Mizuta, R. and Kusunoki, S.: Future change in wintertime atmospheric blocking simulated using a 20-
907 km-mesh atmospheric global circulation model, *J. Geophys. Res.*, 114, D12114, [doi: 10.1029/2009JD011919](https://doi.org/10.1029/2009JD011919), 2009.
908

909 Mizielinski, M. S., Roberts, M. J., Vidale, P. L., Schiemann, R., Demory, M.-E., Strachan, J., Edwards, T., Stephens,
910 A., Lawrence, B. N., Pritchard, M., Chiu, P., Iwi, A., Churchill, J., del Cano Novales, C., Kettleborough, J.,
911 Roseblade, W., Selwood, P., Foster, M., Glover, M., and Malcolm, A.: High-resolution global climate modelling: the
912 UPSCALE project, a large-simulation campaign, *Geosci. Model Dev.*, 7, 1629–1640, [doi:10.5194/gmd-7-1629-](https://doi.org/10.5194/gmd-7-1629-2014)
913 [2014](https://doi.org/10.5194/gmd-7-1629-2014), 2014.
914

915 O'Brien, T. A., Collins, W. D., Kashinath, K., Rübel, O., Byna, S., Gu, J., Krishnan, H. and Ullrich, P. A.: Resolution
916 dependence of precipitation statistical fidelity in hindcast simulations, *J. Adv. Model. Earth Syst.*, 8, 976–990, [doi:](https://doi.org/10.1002/2016MS000671)
917 [10.1002/2016MS000671](https://doi.org/10.1002/2016MS000671), 2016.
918

919 O'Reilly, C. H., Minobe, S. and Kuwano-Yoshida, A.: The influence of the Gulf Stream on wintertime European
920 blocking, *Clim. Dynam.*, 47, 1545- 1567, <https://doi.org/10.1007/s00382-015-2919-0>, 2016.
921

922 Prein, A. F. and Gobiet, A.: Impacts of uncertainties in European gridded precipitation observations on regional
923 climate analysis, *Int. J. Climatol.*, 37, 305-327, [doi:10.1002/joc.4706](https://doi.org/10.1002/joc.4706), 2017.
924

925 Prein, A. F., Langhans, W., Fosser, G., Ferrone, A., Ban, N., Goergen, K., Keller, M., Tölle, M., Gutjahr, O., Feser,
926 F., Brisson, E., Kollet, S., Schmidli, J., Van Lipzig, N. P. M., and Leung, R.: A review on regional
927 convection-permitting climate modeling: Demonstrations, prospects, and challenges, *Rev. Geophys.*, 53, 323–361.
928 [doi: 10.1002/2014RG000475](https://doi.org/10.1002/2014RG000475), 2015.
929

930 Prein, A.F., Gobiet, A., Truhetz, H., Keuler, K., Goergen, K., Teichmann, C., Fox Maule, C., van Meijgaard, E., Déqué, M.,
931 Nikulin, G., Vautard, R., Colette, A., Kjellström, E., and Jacob, D.: Precipitation in the EURO-CORDEX 0.11° and 0.44°
932 simulations: high resolution, high benefits?, *Clim. Dynam.* 46, 383-412, doi: 10.1007/s00382-015-2589-y, 2016.
933

934 Pryor, S. C., Nikulin, G., and Jones, C.: Influence of spatial resolution on regional climate model derived wind
935 climates, *J. Geophys. Res.*, 117, D03117, doi:10.1029/2011JD016822, 2012

936 Rianto, C.B., Castro, C.L., Moker, J.M., Jr., Arellano, A.F., Jr., Adams, D.K., Fierro, L.M., Minjarez Sosa, C.M.:
937 Evaluating Forecast Skills of Moisture from Convective-Permitting WRF-ARW Model during 2017 North
938 American Monsoon Season. *Atmosphere*, 10, 694, doi:[10.3390/atmos10110694](https://doi.org/10.3390/atmos10110694), 2019
939

940 Roberts, M. J., Vidale, P. L., Senior, C., Hewitt, H. T., Bates, C., Berthou, S., Chang, P., Christensen, H. M.,
941 Danilov, S., Demory, M. E., Griffies, S. M., Haarsma, R., Jung, T., Martin, G., Minobe, S., Ringer, T., Satoh, M.,
942 Schiemann, R., Scoccimarro, E., Stephens, G. and Wehner, M.F.: The benefits of global high-resolution for climate
943 simulation: process-understanding and the enabling of stakeholder decisions at the regional scale.. *B. Am. Meteorol.*
944 *Soc.*, 99, 2341–2359 <https://doi.org/10.1175/BAMS-D-15-00320.1>, 2018.
945

946 Ruti, P. M., Somot, S., Giorgi, F., Dubois, C., Flaounas, E., Obermann, A., Dell’Aquila, A., Pisacane, G., Harzallah,
947 A., Lombardi, E., Ahrens, B., Akhtar, N., Alias, A., Arsouze, T., Aznar, R., Bastin, S., Bartholy, J., Béranger, K.,
948 Beuvier, J., Bouffies-Cloch e, S., Brauch, J., Cabos, W., Calmanti, S., Calvet, J., Carillo, A., Conte, D., Coppola, E.,
949 Djurdjevic, V., Drobinski, P., Elizalde-Arellano, A., Gaertner, M., Gal n, P., Gallardo, C., Gualdi, S., Goncalves, M.,
950 Jorba, O., Jord , G., L’Heveder, B., Lebeaupin-Brossier, C., Li, L., Liguori, G., Lionello, P., Maci s, D., Nabat, P.,
951  nol, B., Raikovic, B., Ramage, K., Sevault, F., Sannino, G., Struglia, M. V., Sanna, A., Torma, C., and Vervatis,
952 V.: Med-CORDEX Initiative for Mediterranean Climate Studies. *B. Am. Meteorol. Soc.*, 97, 1187–1208,
953 <https://doi.org/10.1175/BAMS-D-14-00176.1>, 2016
954

955 Schiemann, R., Demory, M. E., Shaffrey, L. C., Strachan, J., Vidale, P. L., Mizielinski, M. S., Roberts, M. J.,
956 Matsueda, M., Wehner, M. F. and Jung, T.: The resolution sensitivity of Northern Hemisphere blocking in four 25-
957 km atmospheric global circulation models, *J. Climate.*, 30, 337–358, <https://doi.org/10.1175/JCLI-D-16-0100.1>,
958 2017.
959

960 Schiemann, R., Vidale, P. L., Shaffrey, L. C., Johnson, S. J., Roberts, M. J., Demory, M.-E., Mizielinski, M. S., and
961 Strachan, J.: Mean and extreme precipitation over European river basins better simulated in a 25 km AGCM, *Hydrol.*
962 *Earth Syst. Sci.*, 22, 3933-3950, <https://doi.org/10.5194/hess-22-3933-2018>, 2018.
963

964 Seneviratne, S. I., Nicholls, N., Easterling, D., Goodess, C. M., Kanae, S., Kossin, J., Luo, Y., Marengo, J., McInnes,
965 K., Rahimi, M., Reichstein, M., Sorteberg, A., Vera, C. and Zhang, X.: Changes in climate extremes and their
966 impacts on the natural physical environment. In: *Managing the Risks of Extreme Events and Disasters to Advance*

967 Climate Change Adaptation. A Special Report of Working Groups I and II of the Intergovernmental Panel on
968 Climate Change, edited by: Field, C. B., Barros, V., Stocker, T. F., Qin, D., Dokken, D. J., Ebi, K., L. Mastrandrea,
969 M. D., Mach, K. J., Plattner, G.-K., Allen, S. K., Tignor, M. and Midgley, P. M., Cambridge University Press,
970 Cambridge, UK, and New York, NY, USA, pp. 109-230, 2012

971

972 Shields, C. A., Kiehl, J. T., and Meehl, G. A.: Future changes in regional precipitation simulated by a half-degree
973 coupled climate model: Sensitivity to horizontal resolution, *J. Adv. Model. Earth Syst.*, 8, 863–884, doi:
974 10.1002/2015MS000584, 2016.

975

976 Skamarock, W.C.: Evaluating Mesoscale NWP Models Using Kinetic Energy Spectra. *Mon. Wea. Rev.*, 132, 3019–
977 3032, <https://doi.org/10.1175/MWR2830.1>, 2004

978

979 Stott, P. A., Christidis, N., Otto, F. E., Sun, Y., Vanderlinden, J., van Oldenborgh, G. J., Vautard, R., von Storch, H.,
980 Walton, P., Yiou, P. and Zwiers, F. W.: Attribution of extreme weather and climate-related events. *WIREs Clim.*
981 *Change*, 7, 23-41. doi:10.1002/wcc.380, 2016.

982

983 Taylor, K., Williamson, D., and Zwiers, F.: The sea surface temperature and sea-ice concentration boundary
984 conditions for AMIP II simulations, PCMDI Rep. 60, Tech. Rep. 60, PCMDI, 25 pp., available at: [http://www-](http://www-pcmdi.llnl.gov/publications/ab60.html)
985 [pcmdi.llnl.gov/publications/ab60.html](http://www-pcmdi.llnl.gov/publications/ab60.html), 2000.

986

987 Taylor, K. E., Stouffer, R. J. and Meehl, G. A.: An overview of CMIP5 and the experiment design, *B. Am. Meteorol.*
988 *Soc.*, 93, 485498, doi: 10.1175/BAMS-D-11-00094.1, 2012.

989

990 Terai, C. R., Caldwell, P. M., Klein, S. A. Tang, Q. and Branstetter, M. L.: The atmospheric hydrologic cycle in the
991 ACME v0.3 model. *Clim. Dynam.*, 50, 3251- 3279. <https://doi.org/10.1007/s00382-017-3803-x>, 2018.

992

993 Torma, C., Giorgi, F. and Coppola, E.: Added value of regional climate modeling over areas characterized by
994 complex terrain—Precipitation over the Alps, *J. Geophys. Res. Atmos.*, 120, 3957–3972, doi:
995 10.1002/2014JD022781, 2015.

996

997 Van Haren, R., Haarsma, R. J., Van Oldenborgh, G. J. and Hazeleger, W.: Resolution Dependence of European
998 Precipitation in a State-of-the-Art Atmospheric General Circulation Model, *J. Climate.*, 28, 5134–5149, doi:
999 10.1175/JCLI-D-14-00279.1, 2015a.

1000

1001 Van Haren, R., Haarsma, R. J., de Vries, H., van Oldenborgh, G. J., and Hazeleger, W.: Resolution dependence of
1002 circulation forced future central European summer drying, *Environ. Res. Lett.*, 10, 055002, doi:10.1088/1748-
1003 9326/10/5/055002, 2015b.

1004

1005 Vanniere, B., Vidale, P. L., Demory, M.-E., Schiemann, R., Roberts, M. J., Roberts, C. D., Matsueda, M., Terray, L.,
1006 Koenigk, T., Senan, R.: Multi-model evaluation of the sensitivity of the global energy budget and hydrological cycle
1007 to resolution, *Clim. Dynam.*, 52, 6817- 6846, <https://doi.org/10.1007/s00382-018-4547-y>, 2019
1008

1009 Vautard, R., Gobiet, A., Jacob, D., Belda, M., Colette, A., Déqué, M., Fernández, J., García-Díez, M., Goergen, K.,
1010 Güttler, I., Halenka, T., Karacostas, T., Katragkou, E., Keuler, K., Kotlarski, S., Mayer, S., van Meijgaard, E.,
1011 Nikulin, G., Patarcic, M., Scinocca, J., Sobolowski, S., Suklitsch, M., Teichmann, C., Warrach-Sagi, K., Wulfmeyer,
1012 V., Yiou, P. : The simulation of European heat waves from an ensemble of regional climate models within the
1013 EURO-CORDEX project, *Clim. Dynam.*, 41, 2555-2575, doi: 10.1007/s00382-013-1714-z, 2013.
1014

1015 Vautard, R., Yiou, P., Otto, F., Stott, P., Christidis, N., van Oldenborgh, G. J. and Schaller, N.: Attribution of human-
1016 induced dynamical and thermodynamical contributions in extreme weather events, *Environ. Res. Lett.*, 11, 114009,
1017 <https://doi.org/10.1088/1748-9326/11/11/114009>, 2016.
1018

1019 Volosciuk, C., Maraun, D., Semenov, V.A. and Park, W.: Extreme Precipitation in an Atmosphere General
1020 Circulation Model: Impact of Horizontal and Vertical Model Resolutions, *J. Climate.*, 28, 1184–1205,
1021 <https://doi.org/10.1175/JCLI-D-14-00337.1>, 2015.
1022

1023 Vries, H. de, Scher, S., Haarsma, R., Drijfhout, S., and Delden, A. van.: How Gulf-Stream SST-fronts influence
1024 Atlantic winter storms, *Clim. Dynam.*, 52, 5899-5909. <https://doi.org/10.1007/s00382-018-4486-7>, 2019
1025

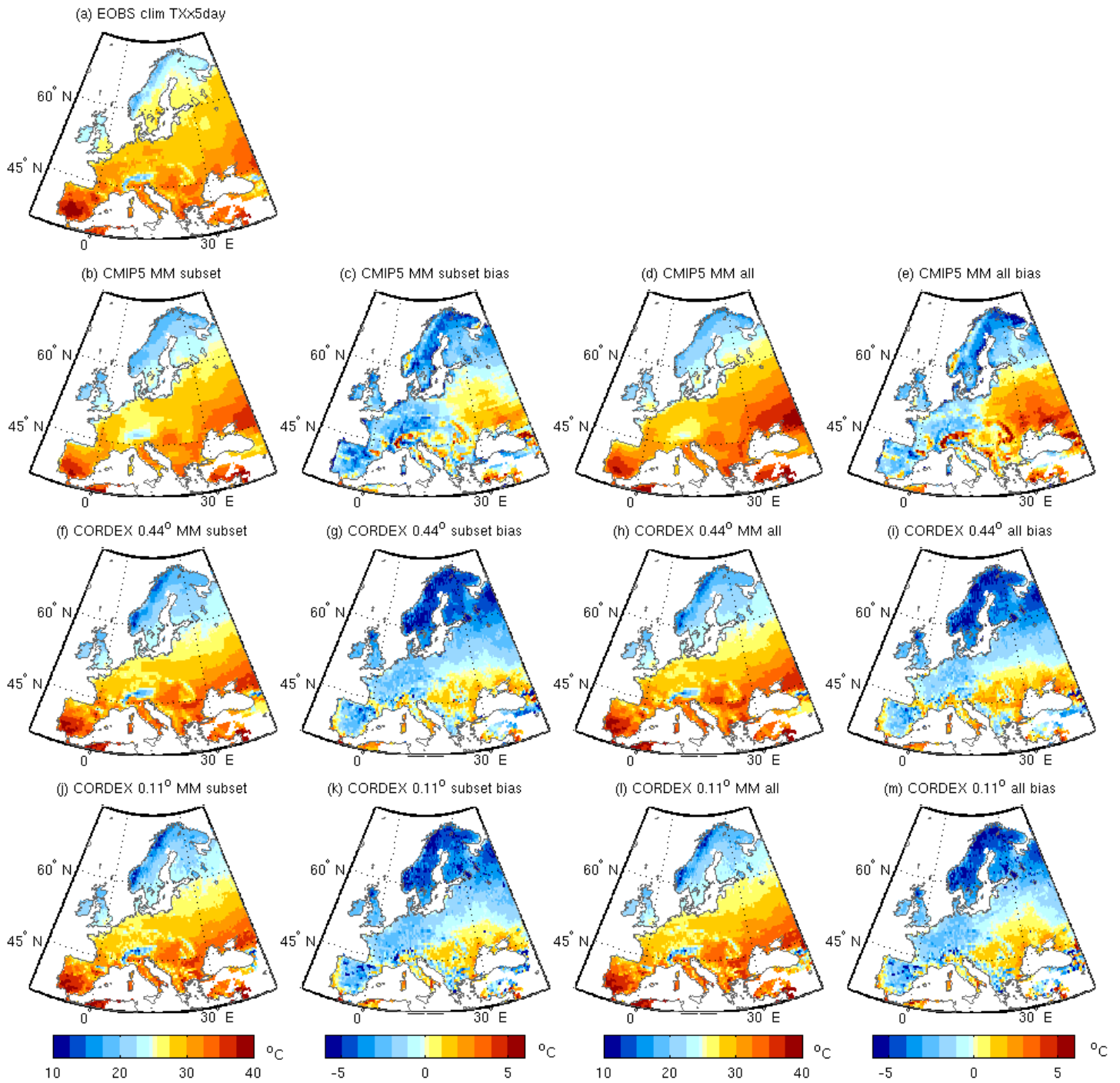
1026 Wehner, M. F., Smith, R. L., Bala, G. and Duffy, P.: The effect of horizontal resolution on simulation of very
1027 extreme US precipitation events in a global atmosphere model, *Clim. Dynam.*, 34, 241-247.
1028 <https://doi.org/10.1007/s00382-009-0656-y>, 2010.
1029

1030 Wehner, M. F., Reed, K. A., Li, F., Prabhat, Bacmeister, J., Chen, C.-T., Paciorek, C., Gleckler, P. J., Sperber, K. R.,
1031 Collins, W. D., Gettelman, A., and Jablonowski, C.: The effect of horizontal resolution on simulation quality in the
1032 Community Atmospheric Model, CAM5.1, *J. Adv. Model. Earth Syst.*, 6, 980–997, doi:10.1002/2013MS000276,
1033 2014.
1034

1035 Willison, J., Robinson, W.A. and Lackmann, G.M.: North Atlantic Storm-Track Sensitivity to Warming Increases
1036 with Model Resolution., *J. Climate.*, 28, 4513–4524, <https://doi.org/10.1175/JCLI-D-14-00715.1>, 2015.
1037

1038 Zappa, G., Shaffrey, L. C. and Hodges, K. I., The Ability of CMIP5 Models to Simulate North Atlantic Extratropical
1039 Cyclones, *J. Climate.*, 26, 5379-5396, doi: 10.1175/JCLI-D-12-00501.1, 2013.
1040

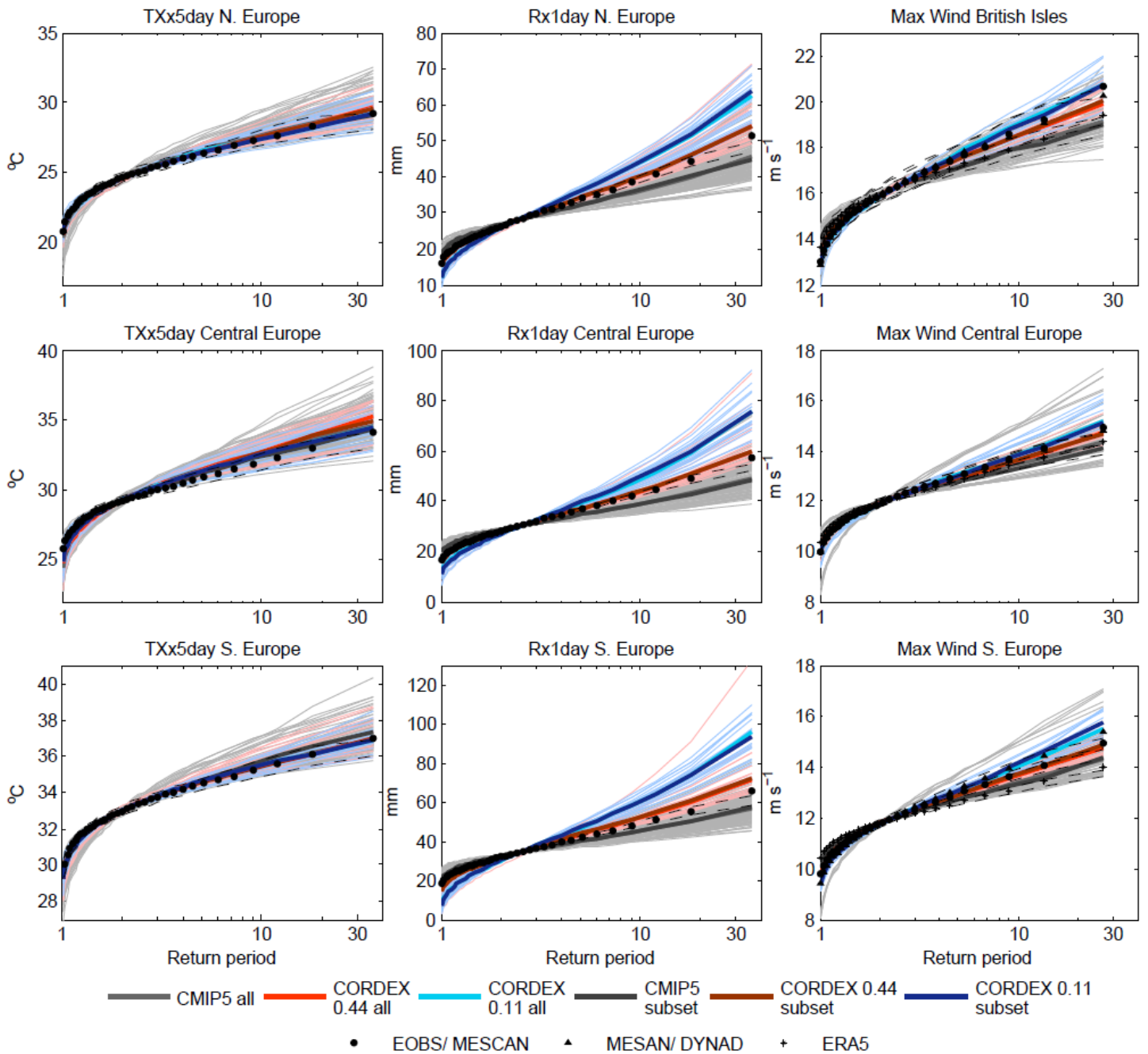
1041 Zhang, X., Alexander, L., Hegerl, G. C., Jones, P., Tank, A. K., Peterson, T. C. Trewin, B. and Zwiers, F. W.:
1042 Indices for monitoring changes in extremes based on daily temperature and precipitation data, Wiley Interdiscip.
1043 Rev., Clim. Chang., 2, 851–870, doi:10.1002/wcc.147, 2011.
1044



1046

1047 **Figure 1: Climatological mean of TXx5day for the period 1970-2005 for (a) EOBS, the multi model mean of the common**
 1048 **subset of models (see Methods) for (b) CMIP5, (f) CORDEX 0.44° and (j) CORDEX 0.11°, (c, g, k) their biases with**
 1049 **respect to EOBS, and (d,e,h,i,j,k) the same for the full ensembles of CMIP5, and CORDEX. Units °C.**

1050

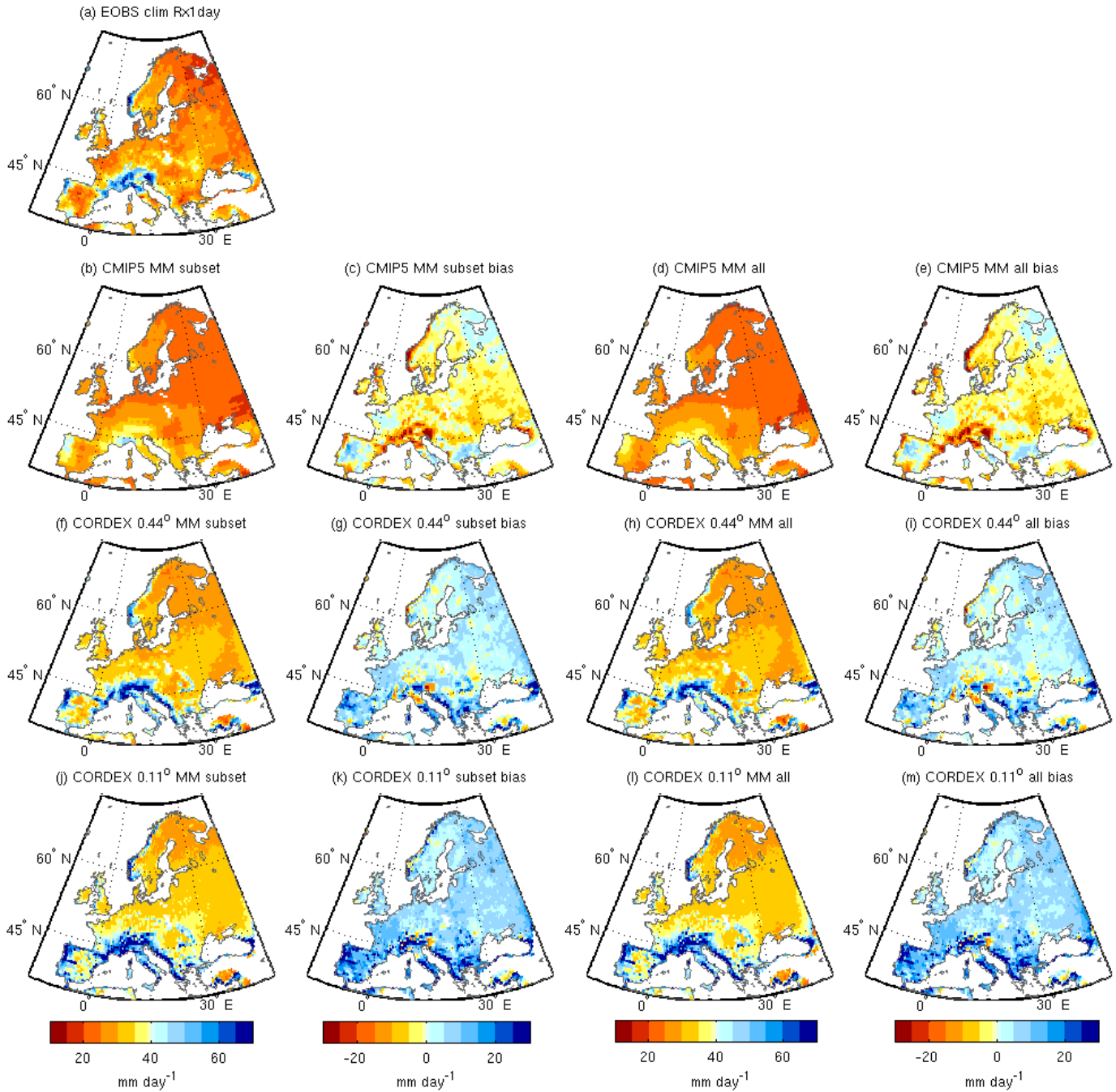


1051

1052 **Figure 2: Return period plots for (left) TXx5day, middle column Rx1day and (right) annual maximum wind, for CMIP5**
 1053 **and CORDEX for Northern Europe (top row (except top left = British Isles)), Central Europe (middle row) and Southern**
 1054 **Europe (bottom row). CMIP5 is shown in grey, CORDEX 0.44° in red and CORDEX 0.11° in blue. Thin lines are**
 1055 **individual ensemble members, thick lines are multi model medians,, lighter shades for the full ensembles, and darker**
 1056 **shades for the subset of models common to CMIP5, and both CORDEX resolutions. Observations are shown in black,**
 1057 **circles for E-OBS temperature and precipitation and MESCAN wind, triangles for MESAN precipitation and**
 1058 **DYNADwind and crosses for ERA5 wind. Confidence intervals based on bootstrapping are shown with dashed lines for**
 1059 **the observations. The time periods considered are 1970-2005 for TXx5day and Rx1day, and 1979-2005 for wind.**

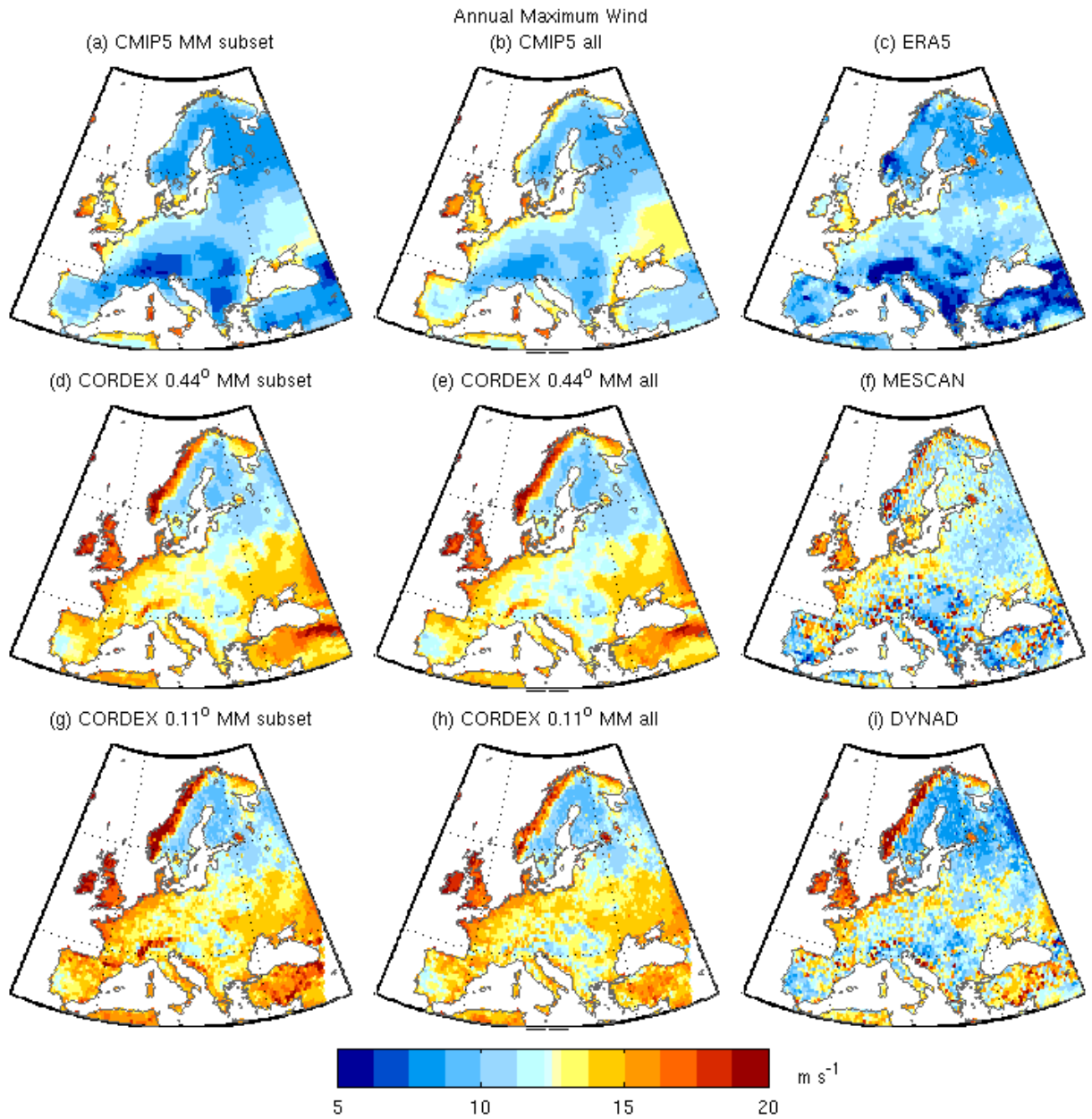
1060

1061

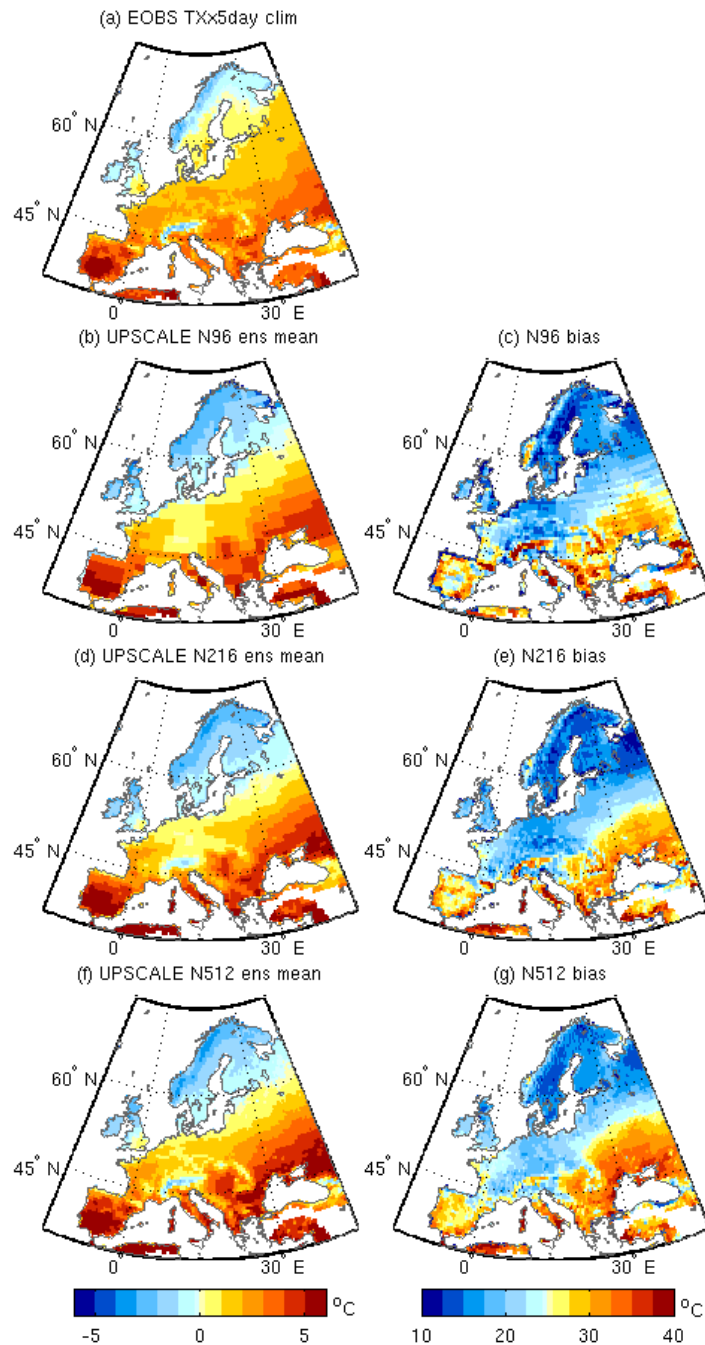


1062

1063 **Figure 3: As for Figure 1 but for the climatological mean of Rx1day. Units mm.**



1064
 1065 **Figure 4: Climatological mean of annual maximum of daily maximum wind for the period 1979-2005 for the multi model**
 1066 **mean of the common subset of models for (a) CMIP5, (d) CORDEX 0.44° and (g) CORDEX 0.11°, (b, e, h) the same for**
 1067 **the full ensembles of CMIP5 and CORDEX, and the observational datasets (c) ERA5, (f) MESCAN (i) DYNAD. Units**
 1068 **meters per second.**



1070 **Figure 5: Climatological mean of Txx5day for the ensemble means of three resolutions of HadGEM3-A (UPSCALE) GCM simulations (left) for the period 1985-2011 and their biases with respect to E-OBS (right). (a) E-OBS, (b, c) N96 (130 km), (d, e) N216 (60 km), (f, g) N512 (25 km). Units °C.**

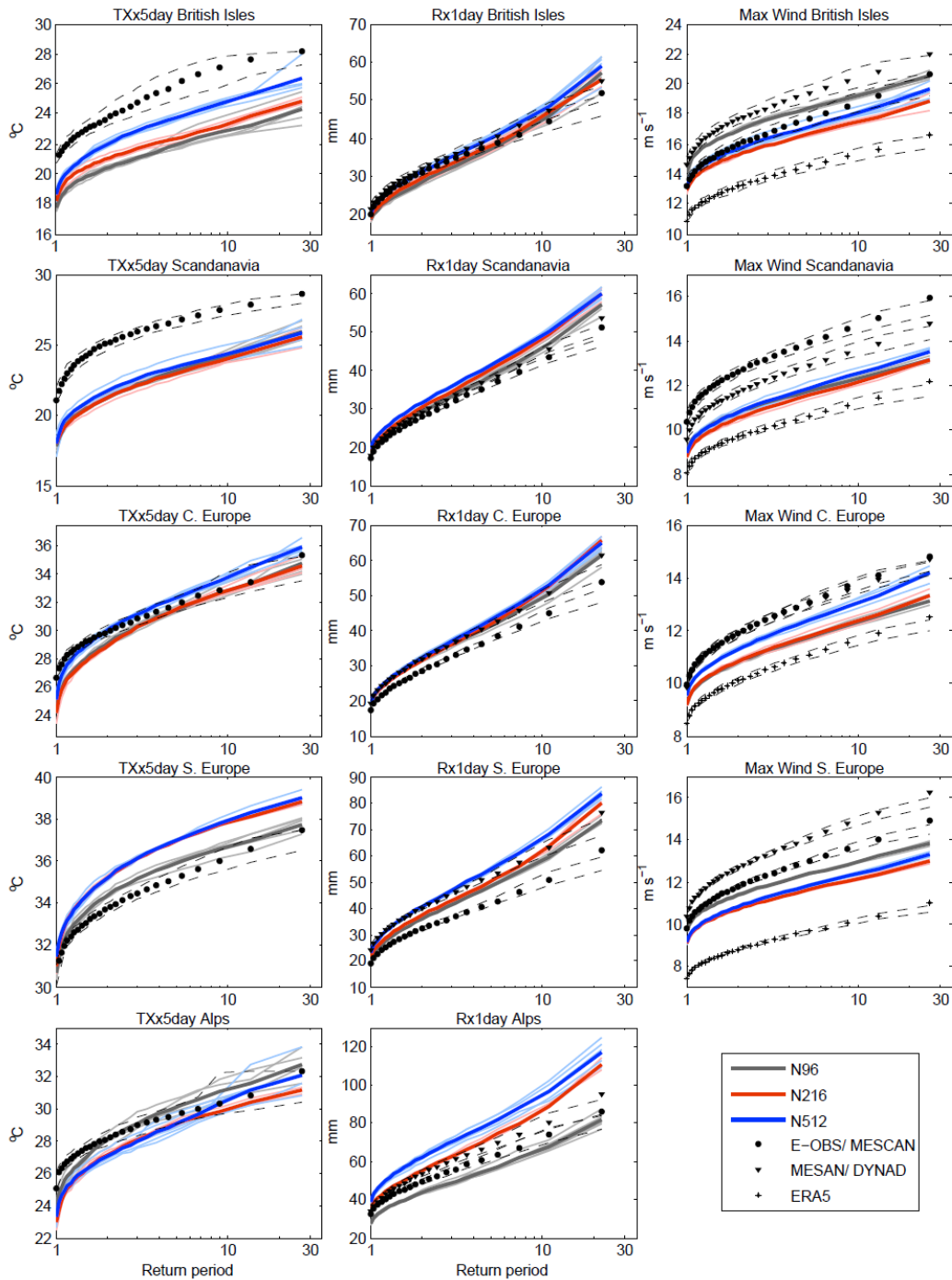
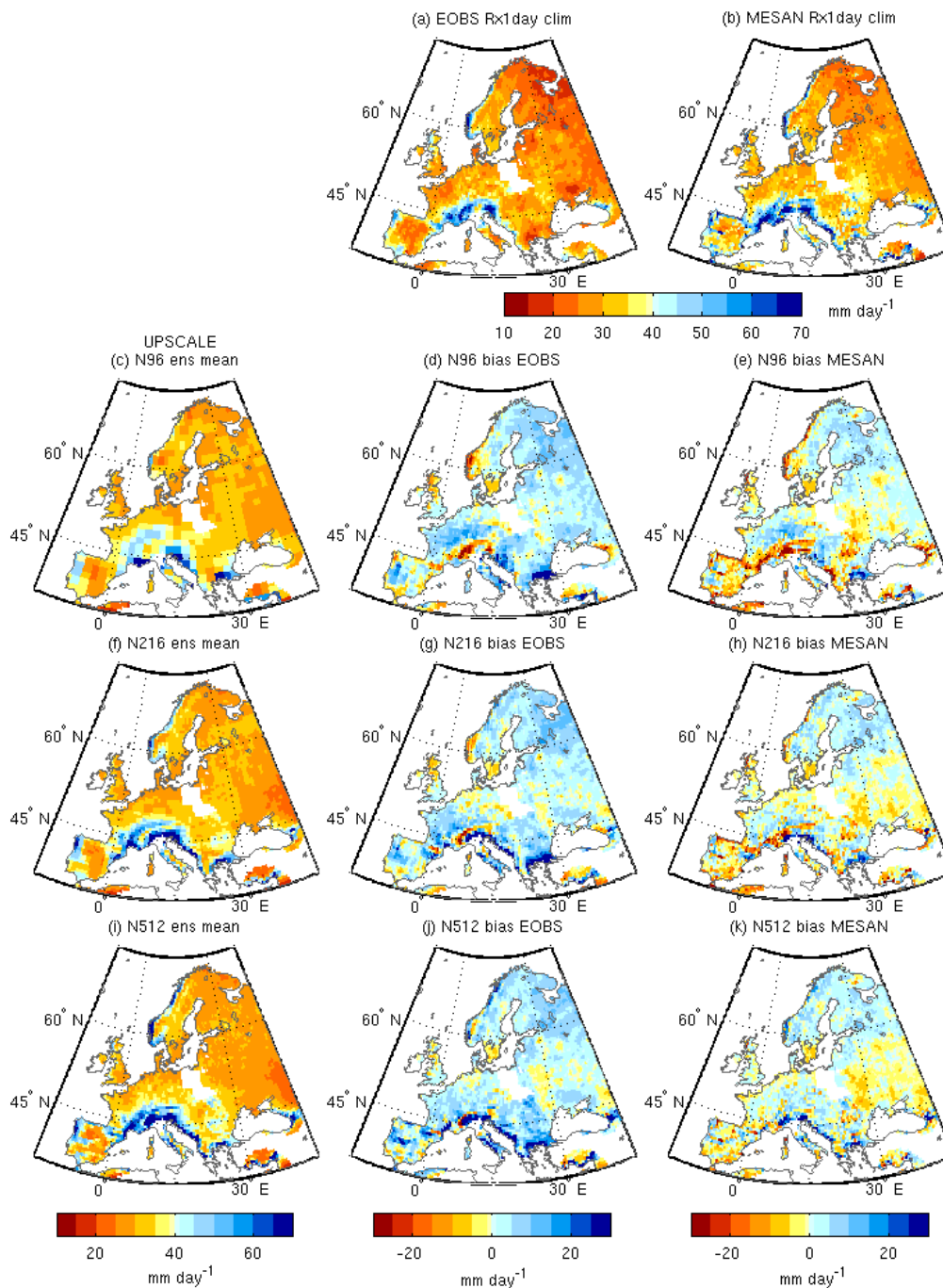


Figure 6: Return period plots for (left) TXx5day, middle column Rx1day and (right) annual maximum wind, for the UPSCALE simulations for (top row) the British Isles, (2nd row) Scandinavia, (3rd row) Central Europe, (4th row) Southern Europe, and (last row) the Alps. N96 is shown in grey, N216 in red and N512 in blue. Thin lines are individual ensemble members, thick lines represent ensemble means. Observations are shown in black, circles for E-OBS and MESCAN, triangles for MESAN and DYNAD, and asterisks for ERA5. Confidence intervals based on bootstrapping are shown with dashed lines for the observations. The time

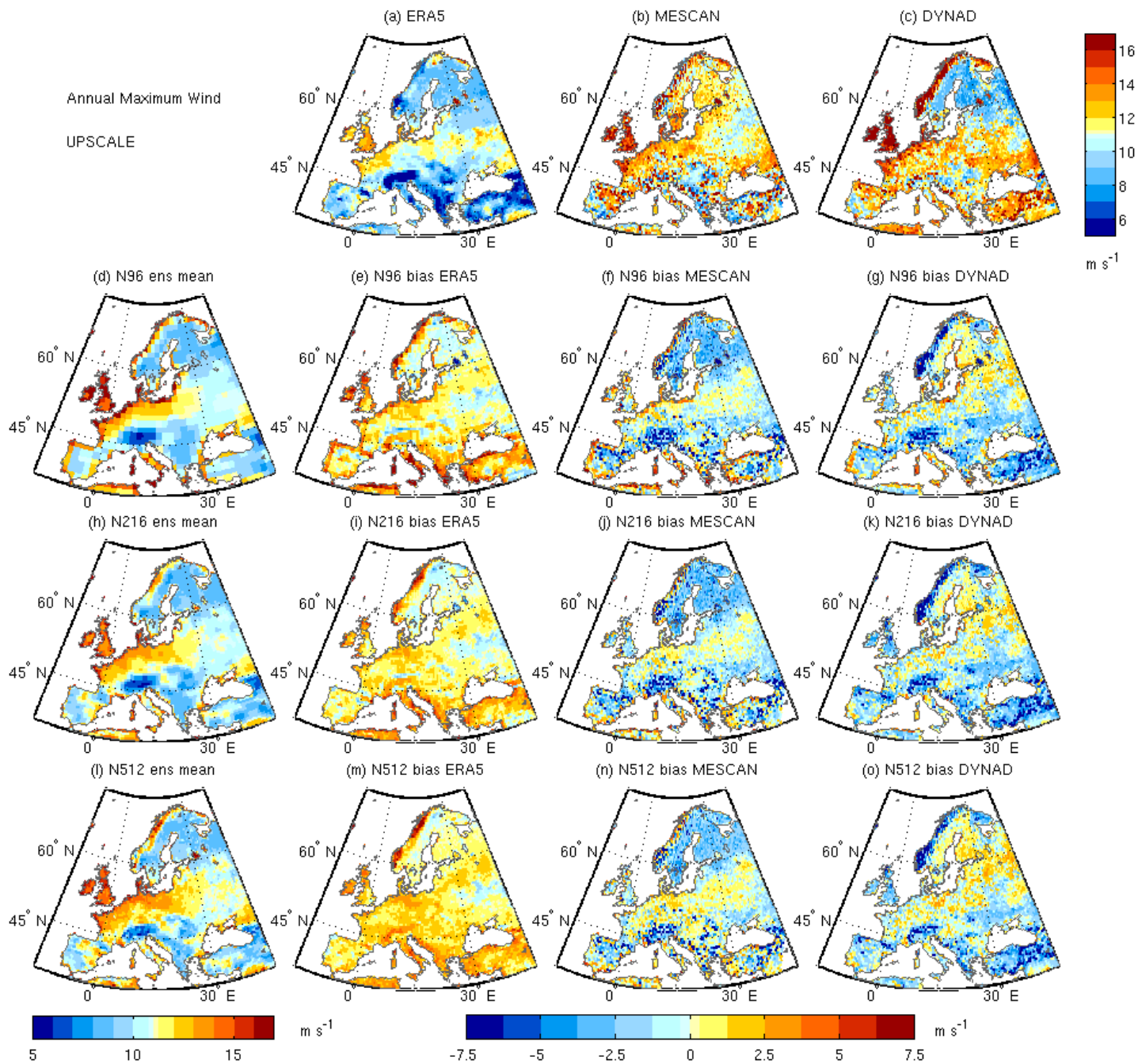
1075

periods considered are 1985-2011 for TXx5day, 1989-2010 for Rx1day, and 1986-2011 for wind. NB: there is no bias adjustment of the climatology (see methods).



1080

Figure 7: Climatological mean of Rx1day for the ensemble means of three resolutions of UPSCALE (left) simulations for the period 1989-2010 and their biases with respect to E-OBS (middle) and the MESAN reanalysis (right). (a) EOBS, (b) MESAN (c-e) N96, (f-h) N216, (i-k) N512. Units mm.



1085 **Figure 8: Climatological mean of annual maximum wind for the ensemble means of three resolutions of UPSCALE (left) simulations for the period 1986-2011 and their biases with respect to the observational datasets ERA5 (left), MESCAN (middle) and MESAN (right). (a) ERA5, (b) MESCAN (c) DYNAD, (d-g) N96, (h-k) N216, (l-o) N512. Units meters per second.**

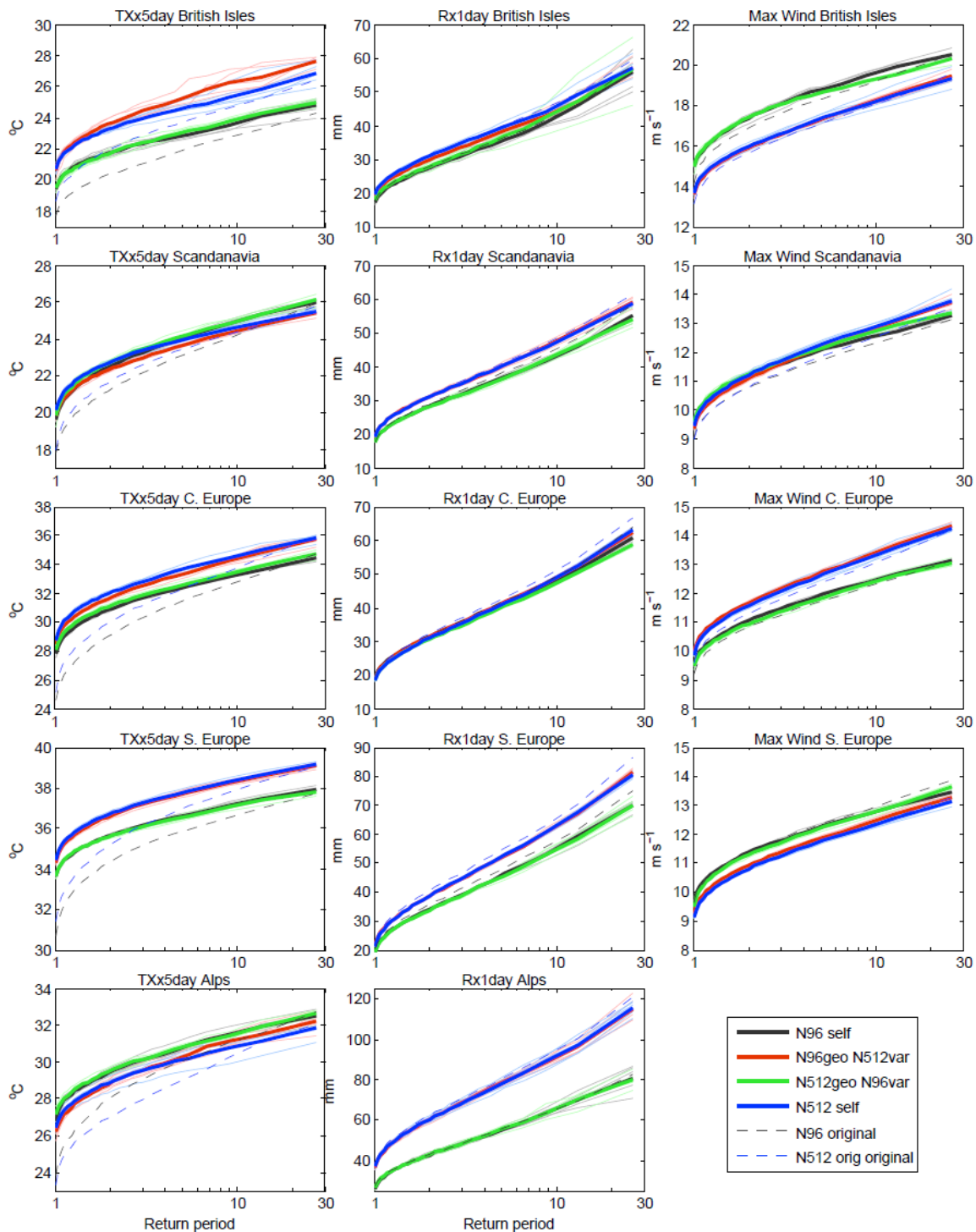


Figure 9: Circulation analogue results. Return period plots for (left) TXx5day, (middle) Rx1day and (right) annual maximum wind for (top) the British Isles, (2nd row) Scandinavia, (3rd row) Central Europe, (4th row) Southern Europe and (5th row) the Alps. Grey represents the N96 self-analogues, blue the N512 self-analogues, red is for N96 circulation with N512 variables (e.g.

1090

precipitation) and green is for N512 circulation with N96 variables. Thin lines represent individual ensemble members, thick lines represent the mean across individual ensemble members. Blue dashed line represents the original N512 ensemble mean results like those shown in Figure 6 (although sometimes based on a different time period), and the grey dashed lines represent the equivalent for the N96 simulations. Results for Txx5day are based on the period 1985-2011, Rx1day 1986-2011, and wind 1986-2011.